Molecular Biology of the Cell
Vol. 15, 481–496, February 2004

The EF-Hand Ca^{2+}-binding Protein p22 Plays a Role in Microtubule and Endoplasmic Reticulum Organization and Dynamics with Distinct Ca^{2+}-binding Requirements

Josefa Andrade, Hu Zhao, Brian Titus, Sandra Timm Pearce, and Margarida Barroso

Albany Medical Center; Center for Cardiovascular Sciences, Albany, New York 12208

Submitted July 17, 2003; Revised October 8, 2003; Accepted November 7, 2003
Monitoring Editor: Reid Gilmore

We have reported that p22, an *N*-myristoylated EF-hand Ca^{2+}-binding protein, associates with microtubules and plays a role in membrane trafficking. Here, we show that p22 also associates with membranes of the early secretory pathway membranes, in particular endoplasmic reticulum (ER). On binding of Ca^{2+}, p22's ability to associate with membranes increases in an *N*-myristoylation-dependent manner, which is suggestive of a nonclassical Ca^{2+}-myristoyl switch mechanism. To address the intracellular functions of p22, a digitonin-based "bulk microinjection" assay was developed to load cells with anti-p22, wild-type, or mutant p22 proteins. Antibodies against a p22 peptide induce microtubule depolymerization and ER fragmentation; this antibody-mediated effect is overcome by preincubation with the respective p22 peptide. In contrast, *N*-myristoylated p22 induces the formation of microtubule bundles, the accumulation of ER structures along the bundles as well as an increase in ER network formation. An *N*-myristoylated Ca^{2+}-binding p22 mutant, which is unable to undergo Ca^{2+}-mediated conformational changes, induces microtubule bundling and accumulation of ER structures along the bundles but does not increase ER network formation. Together, these data strongly suggest that p22 modulates the organization and dynamics of microtubule cytoskeleton in a Ca^{2+}-independent manner and affects ER network assembly in a Ca^{2+}-dependent manner.

INTRODUCTION

An intact microtubule cytoskeleton has been shown to facilitate the assembly of membrane-bound organelles. However, the molecular mechanisms underlying the involvement of microtubules in the organization of membrane-bound organelles are still incomplete. Much of the work in the field has focused on how motor proteins mediate the movement of membrane organelles along microtubules (Allan and Schroer, 1999; Karcher *et al*., 2002), but nonmotor microtubule-associated proteins have also been shown to be involved in organelle assembly and organization (Cassimeris and Spittle, 2001; Schuyler and Pellman, 2001).

A clear dependence on microtubules has been shown for the intracellular distribution of the endoplasmic reticulum (ER) network (Lane and Allan, 1999; Baumann and Walz, 2001), the Golgi apparatus (Thyberg and Moskalewski, 1999), mitochondria (Rappaport *et al*., 1998), synaptic vesicles (Bauerfeind *et al*., 1996), lysosomes (Mithieux and Rousset, 1988), endosomes (Apodaca, 2001), and plasma membrane (Hardham and Gunning, 1978). Several proteins, such Rab GTPases and cytoplasmic linker proteins (CLIPs) modulate the binding of membrane vesicles to microtubules via their interaction with motors (Hammer and Wu, 2002; Perez *et al*., 2002; Howard and Hyman, 2003).

A diverse group of nonmotor-associated proteins has been shown to mediate organelle assembly, movement, organization, and interaction with microtubules. GMAP-210 links Golgi membranes to microtubules, and its overexpression induces microtubule disruption and Golgi fragmentation (Pernet-Gallay *et al*., 2002). Hook3, a microtubule- and Golgi-binding protein, is required for the organization of the Golgi complex (Walenta *et al*., 2001). ch-TOG, the human homolog of XMAP-215, and CLIMP-63, an ER integral membrane protein, act to link microtubules to ER membranes (Charrasse *et al*., 1998; Klopfenstein *et al*., 1998, 2001).

Ca^{2+} controls important cellular processes, such as cell shape and polarity, by affecting microtubule dynamics and membrane trafficking in secretory epithelia and neuronal growth cones (Ashby and Tepikin, 2002; Spira *et al*., 2001). In particular, the early secretory pathway is affected by the efflux of Ca^{2+} from intracellular pools (Ivessa *et al*., 1995; Porat and Elazar, 2000; Chen *et al*., 2002). Consistently, the ER and the Golgi apparatus are well-known Ca^{2+} cellular stores that can release this ion upon stimulation (Pinton *et al*., 1998; Okorokov *et al*., 2001; Petersen *et al*., 2001). However, the Ca^{2+}-binding proteins mediating the Ca^{2+} effects on membrane trafficking and microtubule functions within the secretory pathway are not well characterized.

Article published online ahead of print. Mol. Biol. Cell 10.1091/mbc.E03–07–0500. Article and publication date are available at www.molbiolcell.org/cgi/doi/10.1091/mbc.E03-07-0500.

* Corresponding author. E-mail address: barrosm@mail.amc.edu.

Abbreviations used: ER, endoplasmic reticulum; myr-p22, N-myristoylated bacterially expressed p22; myr-p22-E134A, bacterially expressed N-myristoylated EF-3 Ca^{2+}-binding mutant; p22-rec, non-myristoylated bacterially expressed p22; APpep2 antibodies, affinity-purified antibodies against an unique p22 peptide, pep2; APp22 antibodies, affinity-purified antibodies against full-length p22.

Regulatory EF-hand proteins undergo global conformational changes upon binding of Ca^{2+} and can act as sensors that transduce Ca^{2+} signals to downstream effectors (Ikura, 1996; Nelson and Chazin, 1998). EF-hand proteins, such as calmodulin and neuronal calcium sensor proteins, have been shown to be involved in membrane trafficking (Porat and Elazar, 2000; Pryor *et al*., 2000; Peters *et al*., 2001; Mora *et al*., 2002; Pan *et al*., 2002; Koizumi *et al*., 2002) and to associate with microtubules (Ivings *et al*., 2002; Henriquez *et al*., 1996; Krueger *et al*., 1997).

p22, a widely expressed and evolutionary conserved Ca^{2+}-binding protein, is among the less well characterized members of the EF-hand superfamily. p22 is required for membrane traffic in a cell-free assay, which reconstitutes the targeting/docking/fusion of membrane vesicles with plasma membrane (Barroso *et al*., 1996), and associates with microtubules during interphase and mitosis (Timm *et al*., 1999). Moreover, p22 is *N*-myristoylated and undergoes conformational changes upon binding physiological concentrations of Ca^{2+} (Barroso *et al*., 1996). p22 has been shown to bind NHE-1, a ubiquitous Na/H^+ exchanger (Lin and Barber, 1996; Pang *et al*., 2001), and to inhibit the phosphatase activity of calcineurin (Lin *et al*., 1999), suggesting that p22 possesses multiple cellular functions, as shown for calmodulin and calcineurin B.

Here, we show that p22 associates with membranes of the early secretory pathway, predominantly with the ER network. A nonclassical Ca^{2+}-myristoyl switch is suggested to modulate the p22–membrane association. A digitonin-based "bulk microinjection" assay was used to show that p22 plays a role in microtubule organization and dynamics and ER network formation with distinct Ca^{2+}-binding requirements.

MATERIALS AND METHODS

Preparation of Bacterially Expressed Wild-Type and Mutant p22 Proteins

Several modifications have been made to the previously described bacterial expression and purification of p22 proteins (Timm *et al*., 1999). To generate N-myristoylated proteins, yeast *N*-myristoyl transferase and wild-type p22 or p22-E134A, a Ca^{2+}-binding mutant of the third EF-hand (EF-3) that cannot undergo Ca^{2+}-mediated conformational changes (Barroso *et al*., 1996; Timm *et al*., 1999), were coexpressed in BL21-pLysS in the presence of myristic acid. Nonmyristoylated p22 (p22-rec) was expressed in bacteria in the absence of *N*-myristoyl transferase. After isopropyl β-D-thiogalactoside induction, bacteria were lysed according to manufacturer's instructions (EMD Biosciences, Novagen, Wisconsin, WI). To purify p22 proteins, total lysates were fractionated by DEAE ion exchange chromatography using a 50–500 mM KCl gradient, followed by hydrophobic phenyl-Sepharose chromatography. The *N*-myristoylated wild-type p22 (myr-p22) was bound to the phenyl-Sepharose column in the presence of 10 mM Ca^{2+}, eluted with 10 mM EDTA, and dialyzed against TDE (20 mM Tris-HCl pH 8.0, 1 mM dithiothreitol, 0.5 M EDTA). Because p22-rec and N-myristoylated p22-E134A (myr-p22-E134A) do not show strong affinity toward phenyl-Sepharose in the presence of Ca^{2+} (our unpublished data), these proteins were purified by binding to a phenyl-Sepharose column in the presence of 1 M ammonium sulfate followed by elution with a decreasing 1–0 M ammonium sulfate gradient. Then, fractions containing p22-rec or myr-p22-E134A were dialyzed against TDE buffer and run through a gel filtration Superdex-75 column. All bacterially expressed p22 proteins were kept in TDE and showed 80–95% purity and the expected molecular weight by SDS-PAGE and immunoblot analysis (Figure 4B).

Iodixanol Density Gradients

A freshly dissected Sprague-Dawley rat liver was homogenized in 8 ml of 10 mM Tris pH 7.4, 0.85% NaCl by using a Polytron homogenizer. Homogenate was spun at 1,000 × *g* for 5 min, and the pellet was discarded. Three milliliters of postnuclear supernatant was loaded onto a 36-ml 2.6–20% preformed iodyxanol gradient, prepared as per manufacturer's instructions (Optiprep; Invitrogen, Carlsbad, CA). Sample was spun at 130,000 × *g* for 3 h at 4°C by using a Ti45 rotor. Fractions (2 ml) were collected manually from top to bottom. Equal amounts of fractions 1–18 were analyzed by 12% and 7.5% SDS-PAGE, immunoblotted as described previously (Barroso *et al*., 1996), and processed for enhanced chemiluminescence (ECL) chemiluminescence according to the manufacturer's instructions (Amersham Biosciences, Piscataway, NJ). Nonsaturated film exposures of ECL-treated immunoblots were scanned and quantitated using NIH Image version 1.62. Protein concentration was determined for each fraction by using the Bradford assay according to manufacturer's instructions (Bio-Rad, Hercules, CA).

For a better separation between Golgi and ER membranes, confluent 100-mm plates of BHK21 (hamster kidney) cells were washed with ice-cold phosphate-buffered saline (PBS), scraped into homogenization buffer (HB; 250 mM sucrose, 130 mM KCl, 5 mM $MgCl_2$, 25 mM Tris-HCl, pH 7.4), and spun-down at 1500 × *g* for 10 min. The cell pellet was resuspended into 500 μl of HB and passed 50 times through a 25-gauge syringe. Nuclei and unbroken cells were pelleted at 14,000 × *g* for 5min, and the supernatant further centrifuged at 105,000 × *g* for 1 h in a tabletop centrifuge (Beckman Coulter, Fullerton, CA) by using a TLA 100.3 rotor. The resulting pellet, representing the total membrane fraction, was resuspended into 500 μl of HB. The total membrane fraction was layered on top of a step gradient composed of 1 ml of 15%, 1 ml of 17.5%, 1 ml of 20%, 1 ml of 25%, and 500 μl of 40% iodixanol and centrifuged at 100,000 × *g* at 4°C for 1 h by using a SW55Ti rotor (Beckman Coulter). Thirteen fractions (~385 μl) were collected manually from top to bottom and adjusted to 1 mg/ml total protein. Equal amounts of fraction proteins were analyzed by 12% and 7.5% SDS-PAGE and immunoblotting, followed by ECL and quantitation using NIH Image version 1.62.

Preparation of Microsomal Membranes

Isolation of microsomal membrane fractions was performed as described previously (Fullerton *et al*., 1998) with minor modifications. Briefly, Sprague-Dawley rat livers were minced into small pieces with a razor blade and homogenized by using a Polytron homogenizer at a ratio of 1 g tissue/ml 0.25 M sucrose in acetate buffer (100 mM potassium acetate, 3 mM magnesium acetate, 5 mM EGTA, 1 mM dithiothreitol, 10 mM HEPES, pH 7.1) supplemented with a protease inhibitor cocktail (Sigma-Aldrich, St. Louis, MO). The homogenate was spun at 2500 rpm (907 × g_{max}) in a SS-34 rotor for 10 min at 4°C. The supernatant was then centrifuged at 150,000 × *g* for 1 h at 4°C. Microsomal pellets were resuspended in acetate buffer, assayed for protein concentration, aliquoted, frozen on liquid nitrogen, and stored at −80°C.

Membrane Binding Assay

Microsomal membranes were centrifuged at 174,000 × *g* for 30 min and resuspended in PBS to remove traces of cytosol. Then, 30 μg of the prewashed membranes was incubated with 0.25 μg of myr-p22 in 100 μl of PEM (100 mM PIPES pH 6.6, 1 mM EGTA, 1 mM $MgSO_4$) plus protease inhibitor cocktail and 0.2 mg/ml phenylmethylsulfonyl fluoride for 10 min at 37°C in the presence or absence of different amounts of $CaCl_2$. Free Ca^{2+} concentrations were calculated using the program maxC (http//www.stanford.edu/~cpatton/webmaxcS.htm) by using Ca^{2+}/Mg^{2+}/EGTA buffers. Samples were centrifuged at 174,000 × *g* for 30 min. Membrane pellets were resuspended in equal amounts of SDS-PAGE loading buffer and analyzed by SDS-PAGE and immunoblotting by using anti-p22 and anti-calnexin. ECL-treated immunoblots were quantitated using NIH Image version 1.62.

Microtubule–Membrane-binding Bead Assay

A previously described assay to identify molecules that could link membranes to microtubules (Scheel and Kreis, 1998) was dissected into two separated steps to distinguish between the microtubule- and membrane-binding steps. Briefly, 6 × 10^7 DYNABEADS M-280 tosylactivated (DYNAL, Lake Success, NY) were covered with 20 μg of anti-rabbit IgG, followed by the binding of polyclonal anti-tubulin and incubation with 100 μg of taxol-polymerized microtubules in PEMT buffer (100 mM PIPES pH 6.6, 1 mM EGTA, 1 mM $MgSO_4$, 20 μM taxol) for 30 min at 37°C. Microtubule-covered beads were incubated with 500 μg of rat liver cytosol and 12 μg of myr-p22 in PEMT buffer for 30 min at 37°C. Beads were washed with PEMT buffer and incubated for 30 min at 37°C in PEMT buffer with 100 μg of microsomal membranes, prewashed in PBS. Then, beads were washed with PEMT buffer and resuspended in SDS-PAGE loading buffer. Samples were assayed for tubulin, p22, calnexin, and Rab4 by immunoblotting with 12% (tubulin, p22, and Rab4) and 7.5% (calnexin) SDS-PAGE and quantitation by using NIH Image version 1.62.

Cell Culture

BHK21 cells were grown in DMEM containing 10% fetal bovine serum, 1.5 g/l sodium bicarbonate, and 100 μg/ml penicillin and streptomycin. BHK21 cells were transiently transfected with pECFP-ER vector (Clontech, Palo Alto, CA) by using LipofectAMINE 2000 transfection reagent as per manufacturer's instructions (Invitrogen). The expressed enhanced cyan fluorescent protein (ECFP)-ER protein comprises the ECFP; the calreticulin ER targeting sequence cloned at the 5′ end; and the sequence encoding the ER retrieval sequence, KDEL, cloned at the 3′ end. Medium-expressing cells were detected by fluorescence microscopy (BHK-ER cells).

Bulk Microinjection

Cells were plated on 12-mm diameter glass coverslips and allowed to spread overnight. To minimize cytosol depletion (Gravotta *et al*., 1990), coverslips were incubated in 30 μl of CBS buffer (10 mM MES pH 6.1, 138 mM KCl, 3 mM MgCl, 2 mM EGTA, 0.32 M sucrose) plus 20 μM taxol and 10 μg/ml digitonin in the presence of 5 μg of wild-type or mutant p22 proteins or APpep2 antibodies preincubated or not with pep2 peptide. After 10 min at room temperature, the digitonin solution was removed and coverslips transferred to 200 μl of DMEM + 10% fetal bovine serum for 2–4 h at 37°C, to allow the plasma membrane to recover. Then, cells were washed with PBS and fixed in 4% paraformaldehyde. Fixed cells were subjected to immunofluorescence as described below. These conditions yield a bulk microinjection efficiency of 30–40%. LIVE/DEAD viability/cytotoxicity kit was used to determine two parameters of cell viability, intracellular esterase activity and plasma membrane integrity, as per manufacturer's instructions (Molecular Probes, Eugene, OR). As expected, treatment with high concentrations of digitonin (5 mg/ml) abolishes cell viability and plasma membrane integrity (0%; n = 160–280 cells). In contrast, low amounts of digitonin (10 μg/ml) or no treatment have a reduced effect on cell viability and plasma membrane integrity (100–95%; n = 100–400 cells). Percentage of viable cells = number of bright green cells × 100/total number of cells. Percentage of cells with intact plasma membrane = 100 − (number of bright red cells × 100/total number of cells). Differential interference contrast microscopy was used to determine the total number of cells.

Double or Triple-Label Immunofluorescence Confocal Microscopy

BHK21 or BHK-ER cells were fixed with 4% paraformaldehyde and processed for immunofluorescence, as described previously (Timm *et al*., 1999), except that Cy5-, fluorescein isothiocyanate- and/or tetramethylrhodamine B isothiocyanate-labeled secondary antibodies (Jackson ImmunoResearch Laboratories, West Grove, PA) were used. Then, cells were washed briefly in PBS and mounted on glass slides by using ProLong antifade kit mounting reagent (Molecular Probes). Cells were visualized with an Axiovert S100 inverted microscope (Carl Zeiss) coupled to a CARV confocal unit (Atto Bioscience, Rockville, MD) and Hg vapor light source. Images were collected using Openlab software version 3.0.9 (Improvision, Lexington, MA) with an ORCA-ER digital camera (Hamamatsu Photonics, Hamamatsu City, Japan) and filter sets for fluorescein isothiocyanate (484 nm), tetramethylrhodamine B isothiocyanate (555 nm), and Cy5 (650). Image analysis of confocal images was performed using Adobe Photoshop 5.5. To allow intensity comparisons, we used similar conditions to collect and manipulate images within each experiment.

Antibodies

We have produced affinity-purified antibodies against the following p22 peptides: 155–170 residues (APpep1 antibodies) and 96–113 residues (APpep2 antibodies). Both APpep1 and APpep2 antibodies can recognize bacterially expressed and endogenous p22 by immunoblotting (Barroso *et al*., 1996; Timm *et al*., 1999). APpep2 antibodies display a punctate distribution along microtubule tracks in normal rat kidney (NRK) cells, which can be competitively blocked by preincubation with pep2 peptides (Timm *et al*., 1999). Recently, we have generated polyclonal antibodies against full-length p22 (APp22 antibodies) by raising them in rabbits against purified p22-rec. APp22 antibodies were affinity-purified on strips of nitrocellulose containing myr-p22, eluted with 0.1 M glycine pH2.5 for 10 min, neutralized with 1 M Tris, pH 9.5, dialyzed against PBS, and concentrated to a final volume of ~75–100 μl. APp22 antibodies recognize in vitro translated as well as endogenous p22 by immunoblotting but we have been unable to use APp22 antibodies in immunofluorescence assays due to high background levels (our unpublished data). Here, APpep2 and APp22 antibodies were used in immunoblotting to detect recombinant and endogenous p22, whereas APpep2 antibodies were used in immunofluorescence assays. Antibodies against GM130 (*cis*-Golgi matrix) and rab4 (endosomes) were purchased from BD Biosciences PharMingen (San Diego, CA) and GPP130 (*cis*-Golgi membrane) from Covance Research Products (Berkeley, CA). Polyclonals antibodies against calnexin, an ER membrane protein, were purchased from Stressgen Biotechnologies (San Diego, CA). Polyclonal anti-tubulin antibodies were purchased from Biogenesis Inc. (Kingston, NH) to couple taxol-stabilized microtubules to magnetic beads. For microtubule detection, DM1α from Sigma-Aldrich was used in immunofluorescence and immunoblotting assays.

RESULTS

p22 Associates with Membranes of the Early Secretory Pathway

Because p22 has been shown to be involved in membrane trafficking (Barroso *et al*., 1996), we have tested whether p22 associates with membrane-bound organelles. Rat liver postnuclear supernatants were resolved by centrifugation through 2.6–20% preformed iodixanol density optiprep gradients. Enrichment of rab4 (endocytic marker), GPP130 (*cis*-Golgi membrane marker; Linstedt *et al*., 1997), calnexin (ER membrane marker; Schrag *et al*., 2001), and p22 in the different fractions (shown as %/mg protein) was plotted in Figure 1A. Golgi membranes, as defined by the presence of GPP130, were recovered in fractions 9–15, peaking at fraction 13, whereas ER membranes, as defined by the presence of calnexin, were collected in fractions 14–18, peaking at fraction 17. Rab4 was detected in two major peaks, fractions 3–4 and 7–10. Both peaks should comprise endocytic membranes, because rab4 localizes to vesicular and tubular structures of early endosomes and transport vesicles, which have been shown to fractionate at lower density fractions than Golgi and ER membranes, under these fractionation conditions (van der Sluijs *et al*., 1991; Sheff *et al*., 1999; Mohrmann *et al*., 2002).

In Figure 1A, anti-p22 APpep2 antibodies recognize endogenous p22 in two major peaks, fractions 11–13 and fractions 15–18, representing the p22 fractions that are associated with enriched Golgi and ER membranes, respectively. Fraction 14 may contain p22 together with a mix of Golgi and ER membranes. Under these fractionation conditions, only a minor fraction of p22 is found in the cytosol (<5%), whereas the majority localizes to membranes (~15–20% Golgi and ~70–75% ER). Although the endocytic, Golgi, and ER compartments were not completely separated under the gradient conditions used, they were clearly resolved, demonstrating that p22 associates predominantly with membrane-bound organelles of the early secretory pathway, in particular ER membranes.

To specifically address the association of p22 with ER and Golgi membranes in BHK21 cells, microsomal membrane pellets were fractionated on 15–40% discontinuous iodixanol density optiprep gradients. Equal amounts of protein from gradient fractions were analyzed by SDS-PAGE and immunoblotting by using anti-p22 APp22, calnexin, and GM130 (a *cis*-Golgi matrix protein; Nakamura *et al*., 1995) antibodies (Figure 1B, top). Approximately 60% of p22 cofractionates with calnexin-containing fractions (fractions 9–11), which contain 95% of the calnexin pool and only 12% of the GM130. These results suggest that p22 is significantly enriched in ER membranes (Figure 1B, bottom). Approximately 30% of p22 is present in fractions 2–3, which contain the majority of GM130 (~60%) and only 5% of the calnexin pool. These results suggest that p22 is also enriched in Golgi membranes (fractions 2–3). The ratio of p22 associated with ER and Golgi membranes is slightly different in rat liver and BHK21 cells, probably due to minor differences in the ER/Golgi ratio and organization.

To confirm the topology of membrane-associated p22, we subjected microsomal membranes to high salt, alkaline pH (pH 11.5), and detergent extraction. Increasing amounts of KCl as well as extraction with alkaline pH (pH 11.5) or Triton X-114 lead to the release of p22 from microsomal membrane pellets (our unpublished data). These results suggest that p22 behaves as a peripheral membrane-associated protein, tightly associated with the cytosolic surface of microsomal membranes.

Together, our results indicate that in rat liver and BHK21 cells, p22 associates predominantly with enriched ER membranes with a minor p22 fraction codistributing with Golgi membranes.

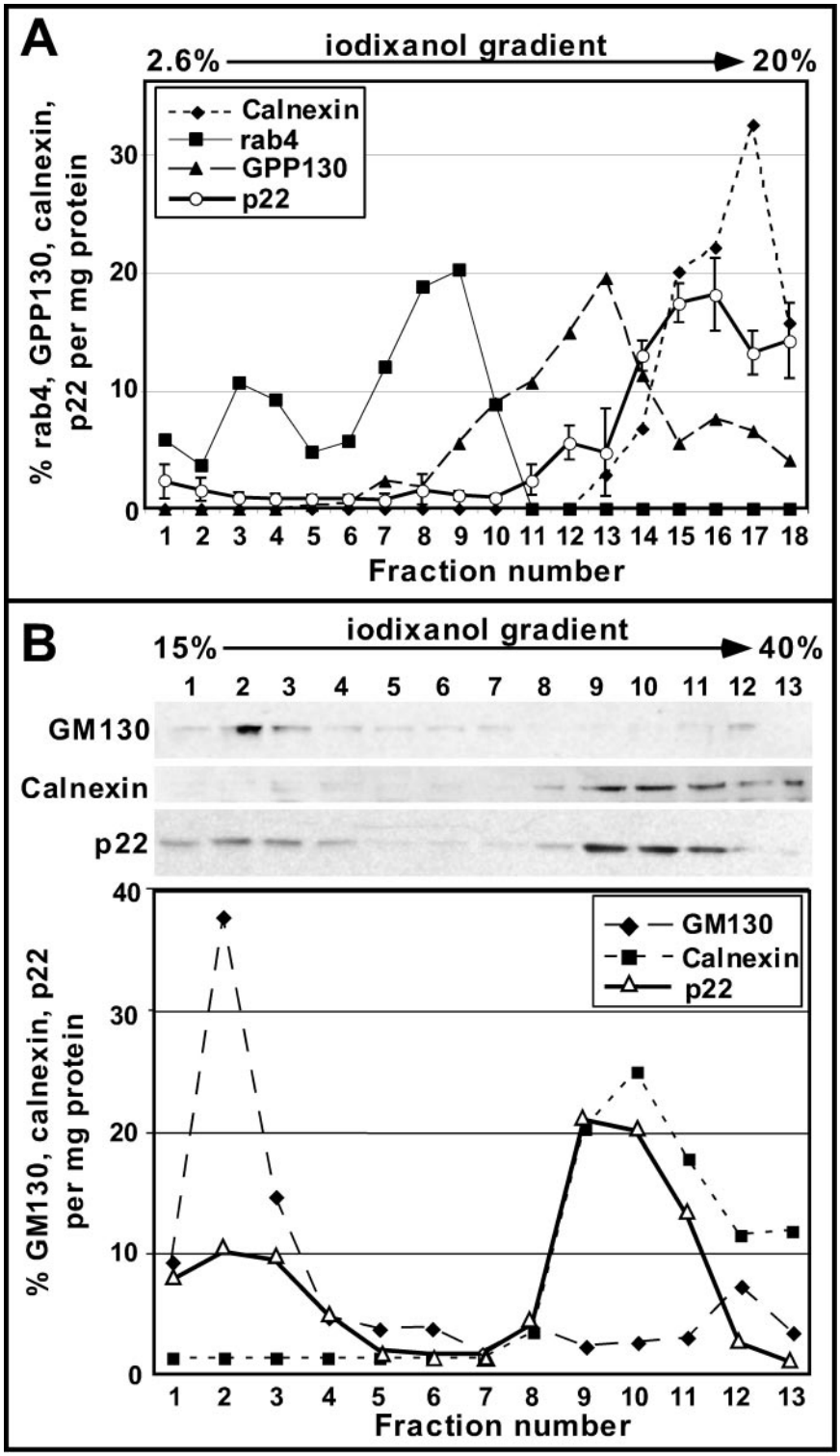

Figure 1. p22 fractionates predominantly with ER membrane fractions using iodixanol gradients. (A) Equal amounts of subcellular fractions were analyzed by SDS-PAGE and immunoblotting by using antibodies against calnexin, rab4, GPP130, and p22. Results were plotted as percentage of rab4, GPP130, calnexin, and p22 per milligram of total protein. p22 data represent mean ± SD of three experiments. (B) Equal protein amounts were analyzed by SDS-PAGE and immunoblotting by using antibodies against GM130, calnexin, and p22. Results were plotted as percentage of GM130, calnexin, and p22 per milligram of total protein.

Characterization of the Intracellular Distribution of p22

As shown previously for NRK cells (Timm *et al*., 1999), BHK21 cells display a typical microtubule pattern by immunofluorescence by using APpep2 antibodies (Figure 2, A–C). Because endogenous p22 distributes to ER- and Golgi-enriched membrane fractions in iodixanol gradients (Figure 1) and myr-p22 associates with microsomal membrane pellets (see below; Figure 4), we assayed whether the staining patterns of p22 and Golgi/ER markers overlap. A clear colocalization between p22 and GM130, a *cis*-Golgi matrix marker, is detected in the perinuclear region of BHK21 cells (Figure 2, D–F). Short tubules containing p22 and GM130 are observed coming off the Golgi apparatus (Figure 2, D–F; arrows). As shown in Figure 2, G–I, and at higher magnification (J–L), the fluorescence staining of ECFP-ER, a soluble ER reporter protein, shows the ER network as tubules that

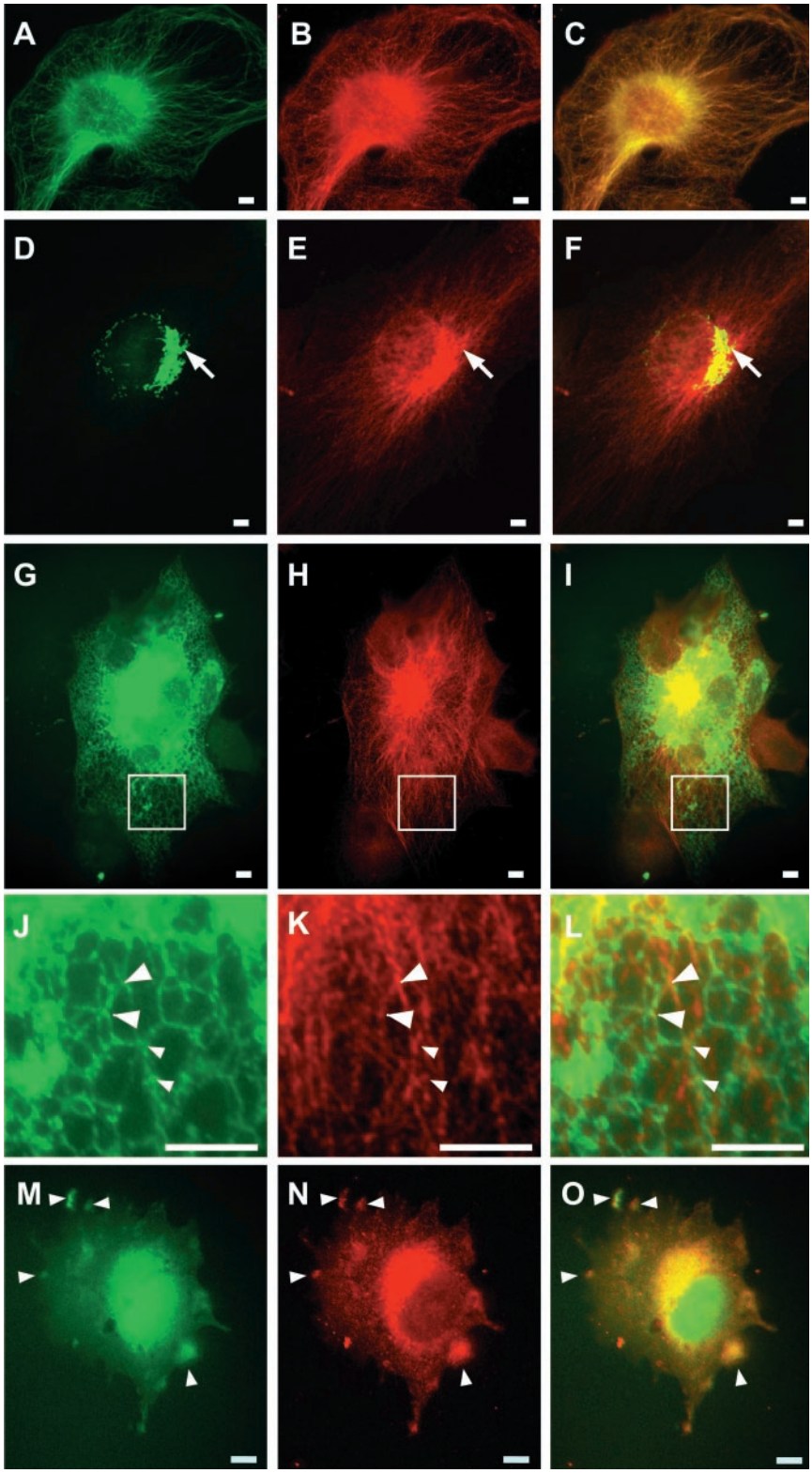

Figure 2. Characterization of the intracellular distribution of p22. BHK (A–F) or BHK-ER (G–O) cells were fixed in 4% paraformaldehyde and processed for immunofluorescence by using antibodies against p22 (B, E, H, K, and N), tubulin (A), and GM130 (D). BHK-ER cells were used for ER staining (G, J, and M). J–L represent magnifications of the regions of interest (square) shown in G–I. In M–O, BHK-ER cells were treated with 5 μg/ml nocodazole for 1 h before cell fixation. Arrows in D–F indicate colocalization between p22 and GM130 structures. Arrowheads in J–O indicate colocalization between p22 and ER structures. Bars, 10 μm.

form a hexagonal reticulum distributed throughout the cell periphery. Similarly, other studies have described the ER as a polygonal network that is anchored to microtubules at the vertices of the polygons (Marsh *et al.*, 2001; Voeltz *et al.*, 2002). Comparison between ER and p22 staining patterns shows ER tubules crossing p22-labeled microtubules and a partial colocalization between the ER network polygonal vertices and p22 (Figure 2, J–L; arrowheads), suggesting that p22 is associated with the ER network. As expected considering the subcellular fractionation results, no colocalization was detected between p22 and rab4 staining patterns (our unpublished data).

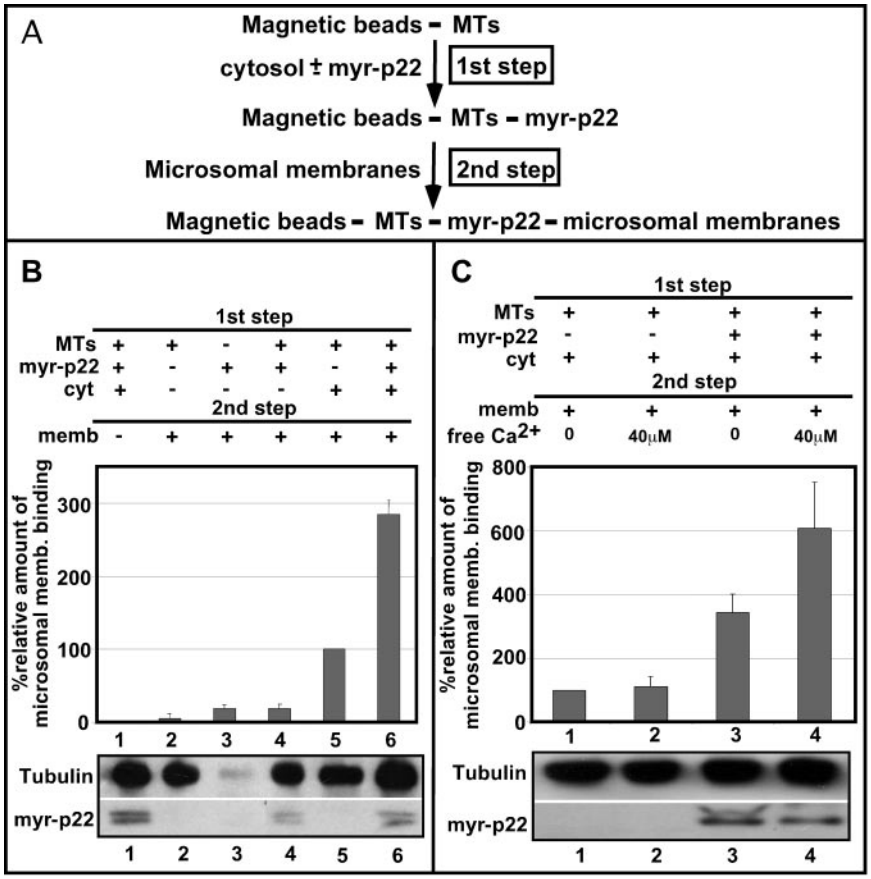

Figure 3. Role of p22 in the interactions between ER membranes and microtubules. (A) Schematic representation of the two-step microtubule-membrane binding assay. (B) Top, DYNABEADS M-280 tosylactivated were covered with taxol-polymerized microtubules (lanes 1 and 2 and 4–6) or not (lane 3) and incubated with or without rat liver cytosol (lanes 1, 5, and 6) and/or myr-p22 (lanes 1, 3, 4, 6) in the first step. Then, beads were incubated with (lanes 2–6) or without (lane 1) microsomal membranes in the second step and immunoblotted with calnexin antibodies. A value of 100% was assigned to the relative binding of microsomal membranes to microtubule-covered beads after incubation with cytosol in the absence of myr-p22 (lane 5). Data represents mean ± SD of three experiments. (B) Bottom, equal amounts of reaction mixtures were analyzed by SDS-PAGE and immunoblotting by using antibodies against tubulin (tubulin) and p22 (myr-p22). (C) Top, microtubule-membrane binding bead assays were performed in the presence of cytosol with (lanes 3 and 4) or without (lanes 1 and 2) myr-p22 in the first step and in the presence (lanes 2 and 4) or absence (lanes 1 and 3) of 40 μM free Ca^{2+} during the second step. A value of 100% was assigned to the relative amount of microsomal membrane binding shown in lane 1, as described above. Data represents mean ± SD of three experiments. (C) Bottom, equal amounts of reaction mixtures were analyzed by SDS-PAGE and immunoblotting by using antibodies against tubulin (tubulin) and p22 (myr-p22).

To address the apparent contradiction between the predominant microtubule localization of p22 by immunofluorescence and the mainly ER/Golgi distribution by subcellular fractionation, we have tested the effect of microtubule depolymerization on the immunofluorescence staining pattern of p22. Our working hypothesis is that the association of p22 with ER membranes may become more evident upon disruption of the microtubule network. BHK-ER cells were treated with 5 μg/ml nocodazole for 1 h and assayed by immunofluorescence by using APpep2 antibodies. Nocodazole-treated BHK-ER cells show the typical retraction of the ER network toward the perinuclear region caused by microtubule depolymerization (Figure 2M). As described previously, in nocodazole-treated cells, p22 displays a diffuse staining with clear punctate structures distributed throughout the cell (Figure 2N; Timm *et al*., 1999). p22 and ER staining patterns colocalize partially in large punctate structures (Figure 2, M–O; arrows), suggesting that at least a fraction of p22 associates with ER membranes after microtubule disruption. In summary, these immunofluorescence results confirm the subcellular fractionation data and suggest the existence of transient interactions between p22, ER, and microtubules in vivo.

p22 Facilitates the Interactions between ER Membrane and Microtubule

Because p22 associates with microtubules and membranes of the early secretory pathway, an interesting hypothesis is that p22 is involved in microtubule-membrane interactions. To test whether p22 can facilitate microtubule–membrane interactions, we have used a slightly modified membrane-microtubule binding assay that was previously used to characterize the ability of CLIP-170 to mediate the interactions of endocytic organelles with microtubules (Scheel and Kreis, 1998). This assay comprises two basic steps, i.e., the association of p22 with microtubules and their subsequent binding to microsomal membranes. The dissection of the original assay in two different steps allows us to separate the binding of p22 to microtubules from their association with membranes. First, magnetic beads were covered with taxol-polymerized microtubules and incubated in the presence or absence of myr-p22 and/or cytosol (Figure 3A, first step). Second, microtubule-covered beads were incubated with microsomal membranes (Figure 3A, second step), washed, and immunoblotted with p22, calnexin, and tubulin antibodies to quantify the amount of p22, ER membranes, and microtubules that are bound to the beads. The tubulin immunoblot confirmed the presence of similar amounts of tubulin covering the magnetic beads in the presence or absence of myr-p22 and/or microsomal membranes (Figure 3B, tubulin). As expected, because p22 associates with microtubules indirectly via a cytosolic factor (Timm *et al*., 1999), the 1st step of the membrane-microtubule binding assay shows a significant increase of p22 bound to microtubules in the presence of cytosol, as demonstrated by p22 immunoblots (Figure 3B, p22). The binding of microsomal membranes to microtubules, as detected by the presence of calnexin bound to microtubule-covered beads, requires the addition of membranes, cytosol, and microtubules, because in the absence of any of these components membrane-microtubule interactions are dramatically reduced (Figure 3B, lanes 1–4). Microtubules preincubated only with cytosol in

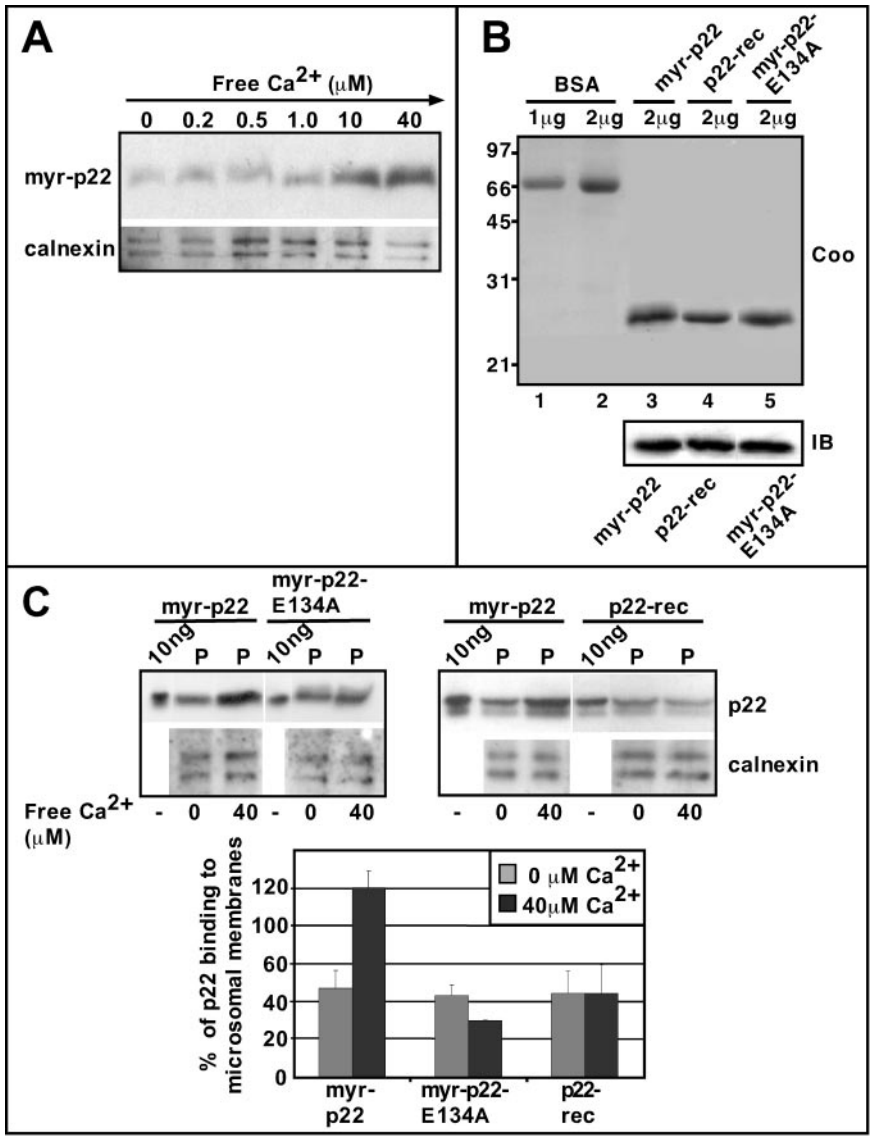

Figure 4. p22 associates with microsomal membranes in a Ca^{2+}-dependent manner. (A) Microsomal membranes were incubated with myr-p22 in the presence of increasing concentrations of free Ca^{2+}, ranging from 0 to 40 μM, and repelleted. Equal amounts of membrane pellets were analyzed by SDS-PAGE and immunoblotting by using p22 (myr-p22) and calnexin (calnexin) antibodies. (B) Bovine serum albumin (BSA) (lanes 1 and 2) and myr-p22 (lane 3), p22-rec (lane 4), and myr-p22-E134A (lane 5) were analyzed by SDS-PAGE and stained with Coomassie Blue (Coo). Equal amounts of myr-p22, p22-rec, and myr-p22-E134A were analyzed by immunoblotting by using antibodies against p22 (IB). (C) Top, microsomal membranes were incubated with myr-p22, myr-p22-E134A, or p22-rec in the presence or absence of 40 μM of free Ca^{2+}. Equal amounts of membrane pellets (P) were compared with the total amount of myr-p22, p22-rec, and myr-p22-E134A (10 ng) added to the assay and analyzed by SDS-PAGE and immunoblotting by using p22 (myr-p22) and calnexin (calnexin) antibodies. (C) Bottom, immunoblots were quantitated as described in MATERIALS AND METHODS. One hundred percent of p22 binding to microsomal membranes would indicate that 100% of the myr-p22 added to the assay was found associated with membranes. Data represents mean ± SD of three experiments.

the 1st step support a basal microsomal membrane binding, which corresponds to a relative value of 100% (Figure 3B, lane 5). The addition of myr-p22 increased to ~300% the amount of ER membranes that are found associated with microtubule-covered beads (Figure 3B, lane 6). Our data suggest that p22 plays a role in the interactions of ER membranes with microtubules.

Our next step was to test whether the p22-dependent microtubule-membrane association is regulated by Ca^{2+}. Similar amounts of tubulin and p22 were found covering the magnetic beads in the presence or absence of 40 μM Ca^{2+} (Figure 3C, tubulin and p22). As described above, basal microsomal membrane binding in the presence of microtubule-bound cytosolic proteins corresponds to a relative value of 100% (Figure 3C, lane 1). In the absence of myr-p22, 40 μM free Ca^{2+} did not affect the amount of microsomal membranes associated with microtubules (Figure 3C, lane 1–2). In contrast, in the presence of p22, addition of 40 μM free Ca^{2+} increased to 600% the amount of membrane associated with microtubules (Figure 3C, lane 1 versus 4) compared with an increase to 300% obtained in the absence of Ca^{2+} (Figure 3C, lane 1 versus 3).

N-Myristoylation and Ca^{2+}-mediated Conformational Changes Are Required for the Ca^{2+}-dependent Binding of p22 to Microsomal Membranes

Although p22 facilitates the binding of microsomal membranes to microtubules in a Ca^{2+}-dependent manner, it binds microtubules independently of Ca^{2+} (Timm *et al.*, 1999), suggesting that Ca^{2+} modulates the ability of p22 to associate with microsomal membranes. We have assayed the effect of Ca^{2+} in the p22-membrane association by incubating microsomal membranes with myr-p22 (8 ng of myr-p22/μg membrane proteins) in the presence of increasing amounts of free Ca^{2+} (0–40 μM). After ultracentrifugation, membrane pellets were assayed by SDS-PAGE and immunoblotting by using anti-p22 and anti-calnexin (Figure 4, A and C). Under these conditions, we were unable to detect significant amounts of endogenous membrane-associated p22 (our unpublished data), making this assay suitable to

determine the structural requirements of p22's association with microsomal membrane pellets. Calnexin is detected in all membrane pellets independently of Ca^{2+} levels (Figure 4, A and C, calnexin). In the absence of Ca^{2+} and in the presence of low amounts of free Ca^{2+} (0.2–1 μM), p22 associates with membrane pellets at similar levels ("constitutive" membrane binding) (Figure 4A, myr-p22). However, in the presence of 10 and 40 μM free Ca^{2+}, a significantly larger amount of p22 is found associated with membrane pellets (Figure 4A, myr-p22). At 40 μM free Ca^{2+}, the amount of membrane-bound myr-p22 increased ~2.0–2.5 times over its constitutive membrane binding, suggesting that p22 binds to microsomal membranes in a Ca^{2+}-dependent manner.

To test whether p22 associates with membranes via a Ca^{2+}-myristoyl switch, we have compared the ability of myr-p22 with that of myr-p22-E134A, an *N*-myristoylated EF-3 Ca^{2+}-binding mutant that is unable to undergo Ca^{2+}-mediated conformational changes (Barroso *et al*., 1996; Timm *et al*., 1999), and p22-rec, a nonmyristoylated form of p22 (Barroso *et al*., 1996; Timm *et al*., 1999), to associate with microsomal membranes in the absence or presence of 40 μM free Ca^{2+}. In Figure 4B, Coomassie Blue-stained SDS-PAGE (Coo) and immunoblots with anti-p22 (IB) show highly purified preparations (80–95%) of myr-p22, p22-rec and myr-p22-E134A with the expected molecular weight.

In Figure 4C, the amount of membrane-associated myr-p22 in the absence or presence of 40 μM free Ca^{2+} was compared with the total amount of myr-p22 added to the assay (100%). Thus, we determined that 44.2 ± 11.2% of total myr-p22 associates with membrane pellets in the absence of Ca^{2+}. In the presence of 40 μM free Ca^{2+}, 103.3 ± 9.98% of myr-p22 associates with membrane pellets compared with the total amount of myr-p22 added to the assay. More than 100% values may indicate an increased amount of membrane-associated endogenous p22. In contrast, both myr-p22-E134A and p22-rec show a similar ability to associate with membrane pellets (~30–40%) in the absence or presence of 40 μM free Ca^{2+} (Figure 4C), suggesting that the constitutive membrane association of p22 proteins is not due to nonspecific *N*-myristoylation–dependent aggregation.

In summary, these results suggest that a Ca^{2+}-myristoyl switch modulates the association of p22 with microsomal membranes.

Digitonin-based Bulk Microinjection Protein Delivery Protocol

To assay the role of p22 in vivo, we have used a bulk microinjection protocol to deliver APpep2 antibodies, myr-p22, and myr-p22-E134A, into digitonin-treated cells. Such an approach is essential to analyze the intracellular functions of p22 because overexpression of p22 by using transient transfection generates significant amounts of nonmyristoylated p22, due to the overwhelming of the *N*-myristoylation machinery (our unpublished data), and *N*-myristoylation is required for the p22-microtubule association (Timm *et al*., 1999). Similar protocols have been used to assay the intracellular distribution of neuronal calcium sensor proteins in the presence or absence of Ca^{2+} (McFerran *et al*., 1999; O'Callaghan *et al*., 2002).

The bulk microinjection protocol takes advantage of digitonin's ability to permeabilize the plasma membrane and allow the delivery of proteins into the cells without affecting the remaining aspects of cellular morphology (Fiskum *et al*., 1980). Under our assay conditions, low amounts of digitonin (10 μg/ml) did not affect cell viability and plasma membrane integrity and delivery of 5 μg of labeled $F(ab')_2$ anti-mouse IgG fragments into digitonin-treated cells did not affect the organization, intensity, and distribution of microtubule cytoskeleton, ER, Golgi apparatus, and endosomes (our unpublished data). These results suggest that if cytosol leakage occurs at all, it should be minimal 2–4 h after digitonin treatment. Here, this digitonin-based bulk microinjection protocol was used to deliver antibodies and recombinant proteins in a quick and efficient manner, without interfering with the morphology of the microtubule cytoskeleton and organelles of the early secretory pathway.

Bulk Microinjection of APpep2 Antibodies Disrupts the Organization of Microtubule Cytoskeleton

To examine the effect of APpep2 antibodies on the organization of the microtubule cytoskeleton, cells were fixed and processed for immunofluorescence at 2 h or 4 h postdigitonin treatment. As shown in Figure 5, A and D, the APpep2 antibodies are found distributed throughout the cytosol at 2 h postdigitonin. Cells containing detectable amounts of APpep2 antibodies display significant disruptions in their microtubule array (Figures 5B and 7E). An enlarged region of interest shows fragmented microtubules that are distributed randomly throughout the cell (Figure 5E). Cells bulk microinjected with APpep2 antibodies also show a dramatic decrease in the intensity of microtubules, in particular in the perinuclear region, compared with that of non-bulk microinjected neighboring cells (Figure 5, A–C). Although there was a significant decrease in microtubule polymer staining, there was little to no tubulin staining in the cytoplasm of cells containing detectable APpep2 antibodies at 2 h postdigitonin, in comparison with nonmicroinjected cells (Figure 5B). A similar phenomenon was detected in cells overexpressing XKCM1, a microtubule-destabilizing protein (Kline-Smith and Walczak, 2002). Furthermore, the entire microtubule network was abolished in cells containing detectable APpep2 antibodies at 4 h postdigitonin (Figure 5, M–O).

Because only a reduced amount of soluble tubulin can be detected in APpep2-bulk–microinjected cells, fluorescence intensity measurements of immunostained microtubules at 2 h postdigitonin were used to estimate microtubule polymer levels, as described previously (Kline-Smith and Walczak, 2002). The average fluorescence intensity level of microtubules was measured by collecting three to four regions of interest (ROIs) from nonsaturated areas of the microtubule network of several cells bulk-microinjected with APpep2 antibodies (n = 26; ROIs = 86) and compared them with nonsaturated ROIs from non-bulk–microinjected neighboring cells (n = 20; ROIs = 41). The fluorescence intensity of microtubule polymers decreased to 26% in cells bulk microinjected with APpep2 antibodies compared with that of neighboring non-bulk–microinjected cells ($p = 7.42E-19$ using two-tailed *t* test analysis, assuming unequal variances) (Table 1).

Previously, we have shown that preincubation of APpep2 antibodies with pep2 peptide leads to a marked reduction in p22's intracellular staining (Timm *et al*., 1999). Here, bulk microinjection of APpep2 antibodies preincubated with pep2 peptides results in a normal microtubule organization (Figure 5, G–L; pep2-competition). We have assayed the two main indicators of the APpep2-mediated effect on the microtubule cytoskeleton, i.e., microtubule disruption and fragmentation as well as reduction in the fluorescence intensity of microtubule polymers. As shown in Figure 5, J–L, microtubules maintain their orientation and network organization in cells bulk microinjected with APpep2 antibodies preincubated with pep2 peptides compared with those in non-bulk–microinjected neighboring cells. Furthermore, we

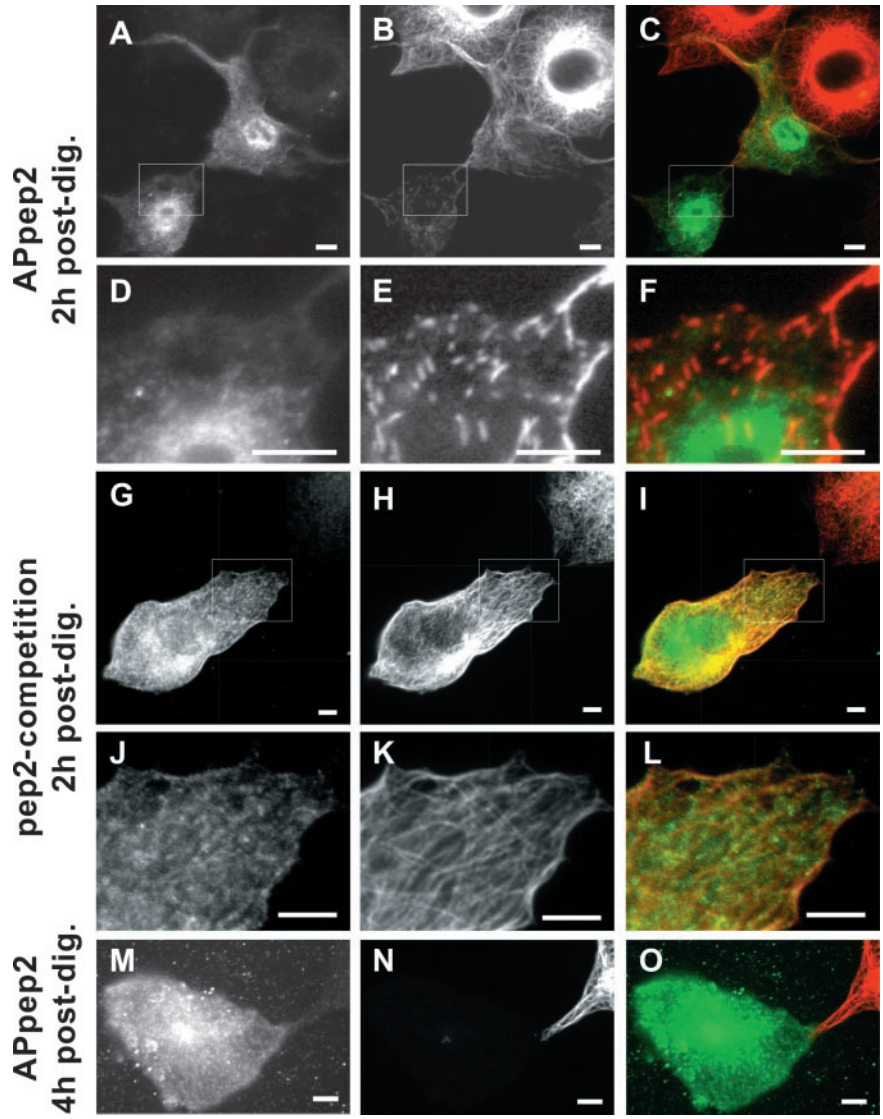

Figure 5. Effect of bulk microinjection of anti-p22 APpep2 antibodies on the organization of the microtubule cytoskeleton. BHK cells were bulk microinjected with APpep2 antibodies (APpep2: A–F and M–O) or APpep2 previously preincubated with pep2 peptide (pep2-competition: G–L) and then allowed to recover at 37°C for 2 h (A–L, 2 h postdig) or 4 h (M–O, 4 h postdig) before fixation. Cells were processed for immunofluorescence by using tubulin antibodies (B, E, H, K, and N). A, D, G, J, and M show APpep2 staining, indicating bulk-microinjected cells. C, F, I, L, and O represent merged images. D–F and J–L are magnifications of the regions of interest shown in A–C and G–I, respectively. Bars, 10 μm.

found only a decrease to 83% in the average fluorescence intensity level of microtubule polymers in cells bulk microinjected with pep2-preincubated APpep2 antibodies (n = 11; ROIs = 33) compared with that of neighboring non-bulk–microinjected cells (n = 12; ROIs = 21) (Table 1). Significantly, there is no statistical difference between these two ROI populations (p = 0.2 by using two-tailed *t* test analysis, assuming unequal variances). These results suggest that the ability of APpep2 antibodies to disrupt the microtubule cytoskeleton is mediated by p22.

Table 1. Fluorescence intensity of microtubule polymers

Bulk microinjection	Fluorescence intensity	t-test non-bM.I. vs. bM.I.
Non-bM.I.	100%	N.A.
APpep2 bM.I.	26%	p = 7.42E-19
pep2-competition bM.I.	83%	p = 0.2

N.A., nonapplicable; bM.I., bulk microinjection.

Bulk Microinjection of myr-p22 or myr-p22-E134A Induces Microtubule Bundling

To complement the APpep2 antibody experiments, we have examined the effect of raising the amount of myr-p22 on the organization of the microtubule cytoskeleton using the digitonin-based bulk microinjection protocol. Cells were bulk microinjected with myr-p22 and processed for immunofluorescence by using APpep2 antibodies at higher dilutions, which were optimized to detect exogenous myr-p22 in bulk-microinjected cells and minimize the detection of endogenous p22. Cells bulk microinjected with myr-p22 display a dramatically rearranged microtubule network, in which several microtubule bundles are found distributed throughout the cell (Figure 6, D–F, arrowheads). p22 is predominantly found associated with bundled microtubules but a minor fraction remains localized to nonbundled microtubules, which show a disorganized pattern (Figure 6D). Nonbundled microtubules display a significantly lower microtubule and p22 staining compared with that of microtubule bundles. As expected, mock-bulk–microinjected cells show a typical microtubule radial organization with no detectable microtubule bundling (Figure 6, A–C).

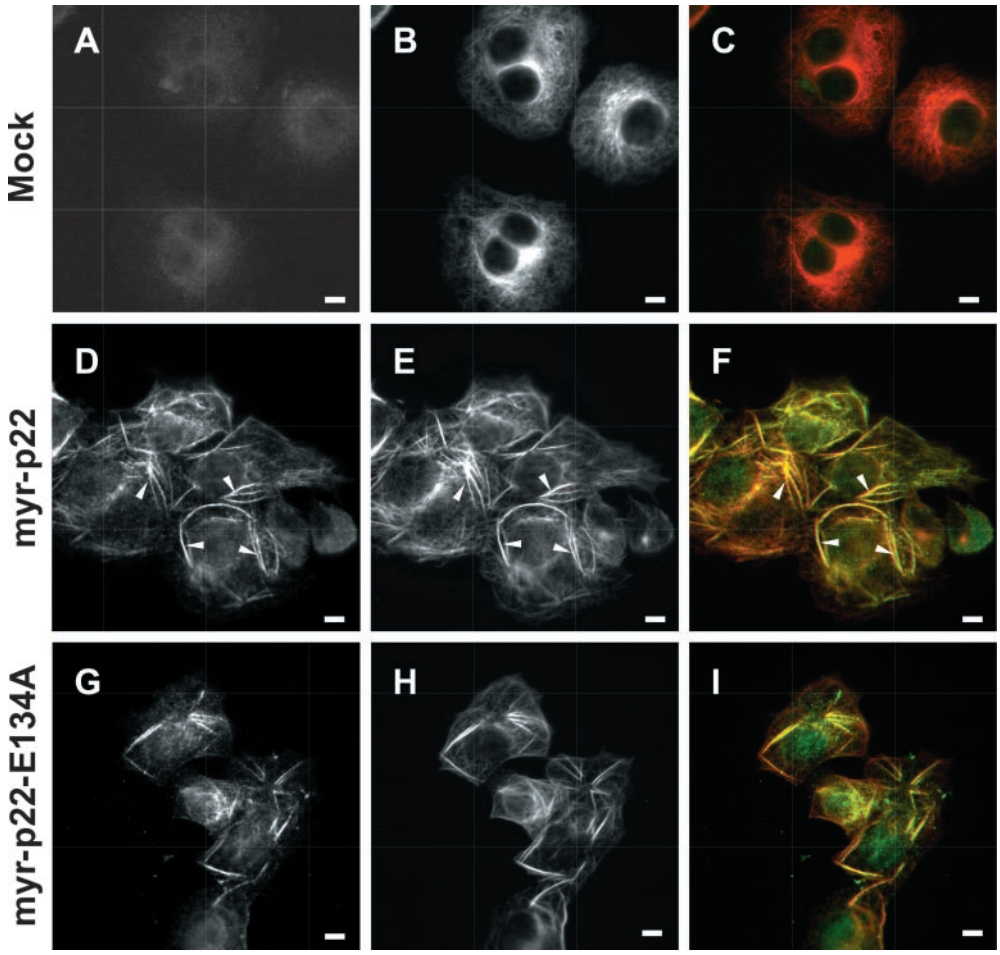

Figure 6. Effect of bulk microinjection of myr-p22 or myr-p22-E134A on the organization of the microtubule cytoskeleton. BHK cells were mock (A–C), myr-p22 (D–F and J–L) or myr-p22-E134A (G–I) bulk microinjected. After 2 h at 37°C, cells were fixed and processed for immunofluorescence by using APpep2 (A, D, and G) and tubulin (B, E, and H) antibodies. C, F, and I represent merged images. Bars, 10 μm. Arrowheads in D–F indicate p22-positive microtubule bundles.

Bulk microinjection of myr-p22-E134A, an EF-3 Ca^{2+}-binding mutant that is unable to undergo Ca^{2+}-mediated conformational changes but still can associate with microtubule pellets (Barroso *et al*., 1996; Timm *et al*., 1999), induces microtubule bundle formation in a similar manner to that of myr-p22 (Figure 6, G–I). Our data suggest that p22 regulates microtubule dynamics and stability in vivo, independently of its ability to undergo Ca^{2+}-induced conformational changes.

Bulk Microinjection of anti-p22 APpep2 Antibodies Induces ER Fragmentation and Vesiculation

Immunofluorescence, subcellular fragmentation, and membrane binding assays suggest that p22 associates with ER membranes. To test the role of p22 on the organization and morphology of the ER network, we have assayed the effect of bulk microinjecting APpep2 or p22 proteins into BHK-ER cells. Cells microinjected with detectable amounts of APpep2 antibodies show a disrupted and highly vesiculated ER (Figure 7, A–C, APpep2). APpep2-positive cells in this experiment also show a dramatic decrease in the intensity of microtubules (our unpublished data). To test the specificity of the APpep2 effect on the ER network, APpep2 antibodies were preincubated with pep2 peptides, as described above. BHK-ER cells bulk microinjected with pep2-preincubated APpep2 antibodies with pep2 showed an ER morphology and distribution undistinguishable from that of non-bulk–microinjected BHK-ER cells (Figure 7, D–F, pep2-competition), indicating that the APpep2-mediated ER vesiculation occurs in a p22-specific manner. These cells also show a normal microtubule network (our unpublished data). In summary, the APpep2 and pep2-competition data suggest a role for p22 in the dynamics and organization of the ER network.

Effect of Bulk Microinjection of myr-p22 and myr-p22-E134A on the Organization of the ER Network

Previously, we have shown that bulk microinjecting myr-p22 into cells induces the formation of microtubule bundles that are positive for p22. To test the hypothesis that p22 is involved in the interaction of microtubules bundles with ER tubules, we assayed whether bulk microinjection of myr-p22 into BHK-ER cells affects the organization of the ER network. As shown in Figure 8A, c and d, cell areas containing microtubule bundles (d) display a rearranged ER network (c), which seems retracted toward the microtubule bundles both from the cell periphery and perinuclear regions (arrowheads). To specifically address the interaction of ER with

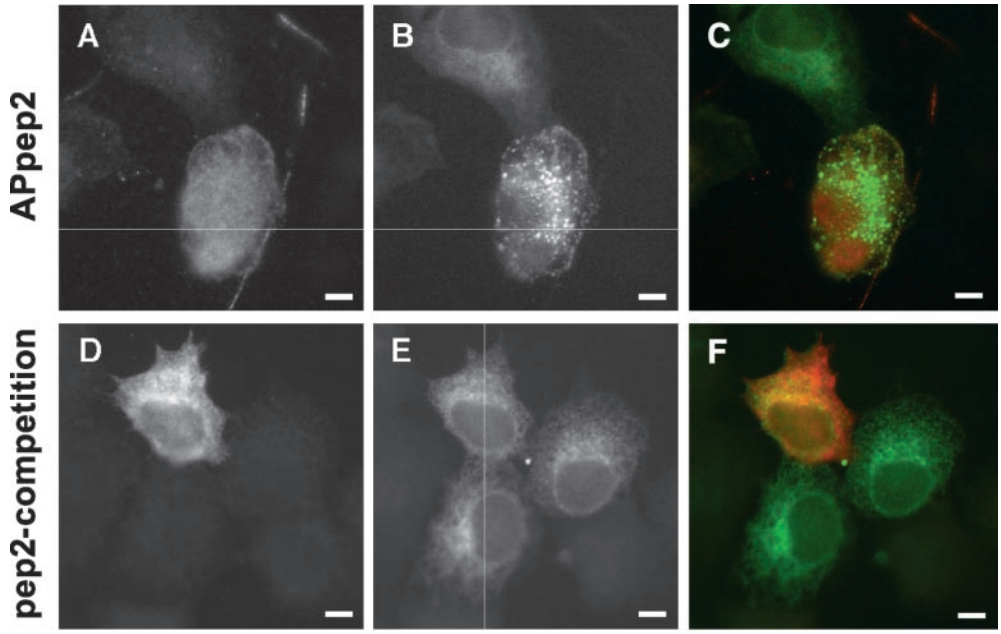

Figure 7. Effect of bulk microinjection of APpep2 antibodies on the organization of the ER network. BHK-ER cells were bulk microinjected with APpep2 (A–C, APpep2) or APpep2 previously preincubated with pep2 (D–F, pep2-competition) and allowed to recover for 2 h at 37°C. Then cells were fixed and processed for immunofluorescence. A and D show APpep2 staining, indicating bulk-microinjected cells. The fluorescence pattern of ECFP-ER protein shows the ER network (B and E). C and F represent the merged images. Bars, 10 μm.

myr-p22–induced microtubule bundles, several lines were drawn from the cell periphery to the perinuclear region crossing one or more myr-p22-induced microtubule bundles (Figure 8A, c and d, lines 6–7). Lines were also drawn in mock-bulk–microinjected cells from the cell periphery to the perinuclear region crossing nonbundled radially organized microtubules (Figure 8A, a and b, lines 1–2). ImageJ software was used to produce plot profiles of these lines, i.e., two-dimensional graphs of the intensities of pixels along the lines within the image. After background subtraction, the x-axis represents the distance along the line (up to 31 μm), and the y-axis corresponds to the normalized pixel grayscale intensity (Figure 8B). In general, for ER staining, 100% corresponds to the highest grayscale intensity detected at the perinuclear region, and 0% corresponds to the lowest grayscale intensity in the extracellular space. For microtubule staining, 0% represents the extracellular space and 100% the microtubule bundles. In Figure 8B, several of these plot profiles are shown for non-bulk–microinjected (1–5 include lines 1 and 2 from Figure 8A and lines 3–5 from other not-shown cells) and myr-p22 bulk microinjected (6–10 include lines 6 and 7 from Figure 8A and lines 8–10 from other not-shown cells) BHK-ER cells. Myr-p22-positive BHK-ER cells show ER structures accumulating at the microtubule bundles (Figure 8B, 6–10), whereas non-bulk–microinjected BHK-ER cells display a steady increase in intensity from the cell periphery to the perinuclear region without significant accumulation at specific microtubules (Figure 8B, 1–5). An overlap between the peak intensities of ER structures and microtubule bundles is detected in myr-p22–positive cells (Figure 8B, 6–10).

Because Ca^{2+}-mediated conformational changes increase the ability of p22 to associate with microsomal membranes (Figure 4) but not with microtubule pellets (Timm *et al.*, 1999), we have tested whether bulk microinjection of myr-p22-E134A alters the organization of the ER. As shown in Figure 8A, c–f, in areas where microtubule bundles can be detected (d and f), there is no significant difference between the ER network of myr-p22–positive cells and that of myr-p22-E134A–positive cells (c and e). Several lines were drawn from the cell periphery to the perinuclear region to cross microtubule bundles in myr-p22-E134A–positive cells (Figure 8A, e–f, lines 11 and 12) and plot profiles were performed as described above (Figure 8B, 11–15 include lines 11 and 12 from Figure 8A and lines 13–15 from other not-shown cells). In myr-p22-E134A–positive cells, the peak intensities of ER structures and microtubule bundles overlap (Figure 8B, 11–15), as described above for myr-p22–positive cells (Figure 8B, 6–10).

The remaining ER network that is localized to bundle-free areas in myr-p22 bulk-microinjected BHK-ER cells is distributed throughout the cell periphery and perinuclear regions, and it seems highly reticulated (Figure 9B), compared with that of neighboring nonmicroinjected cells and of cells bulk microinjected with myr-p22-E134A (Figure 9, A and C). This change in ER structure suggests that raising the intracellular amount of p22 results in an increasingly reticulated/developed ER network. To quantify the degree of ER network formation, we have counted the number of three-way junctions by using confocal microscopy (Figure 9D). The number of three-way junctions was significantly increased by 100% in BHK-ER cells bulk microinjected with myr-p22, compared with nonmicroinjected BHK-ER cells ($p = 7.27E-08$ by using two-tailed t test analysis, assuming unequal variances; $n = 11–20$). This role of p22 in ER network formation occurs in a Ca^{2+}-dependent manner because bulk microinjection of myr-p22-E134A does not increase the number of three-way junctions compared with nonmicroinjected BHK-ER cells (Figure 9D). Actually, introducing myr-p22-E134A into BHK-ER cells results in a slight, but significant, ~15% decrease in the number of three-way ER junctions ($p = 2.87E-03$ by using two-tailed t test analysis, assuming unequal variances; $n = 20–25$). The intracellular distribution of rab 4-positive endocytic structures is similar in cells that are

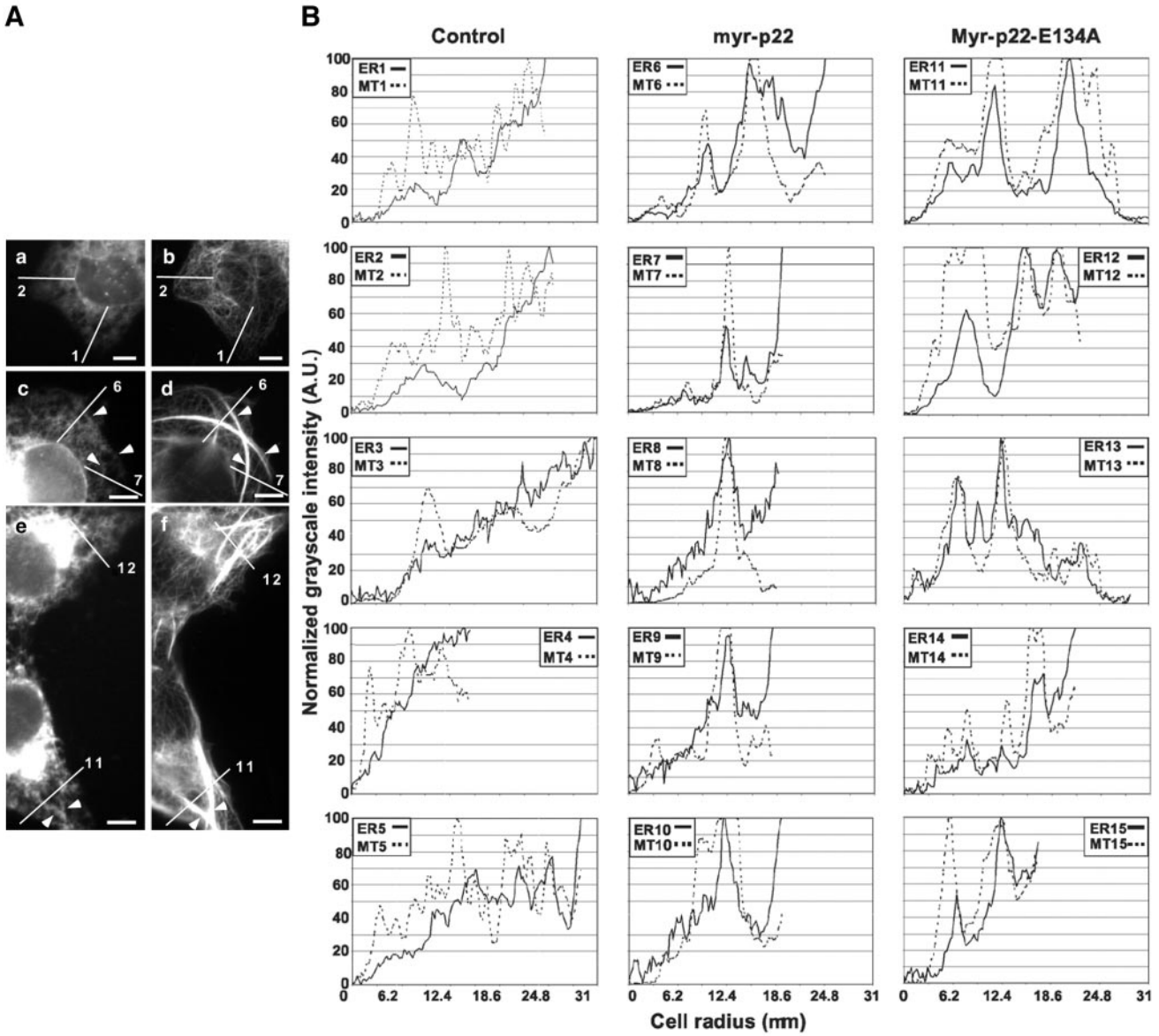

Figure 8. ER structures accumulate at myr-p22–induced microtubule bundles. (A) BHK-ER cells were mock (a and b), myr-p22 (c and d), or myr-p22-E134A (e and f) bulk microinjected, allowed to recover for 2 h and then processed for immunofluorescence by using tubulin antibodies. a, c, and e show the ECFP-ER fluorescence pattern, and b, d, and f show the microtubule staining. Lines were drawn from the periphery to the perinuclear region in mock (lines 1 and 2) and myr-p22 (lines 6 and 7) or myr-p22-E134A (lines 11 and 12) bulk-microinjected cells, and the corresponding plot profiles are shown in B. These lines were made to cross several myr-p22 (lines 6 and 7) or myr-p22-E134A (lines 11 and 12) induced microtubule bundles. Bars, 10 μm. (B) ImageJ software was used to produce plot profiles of the microtubule (MT: dashed lines) and ER (solid lines) networks along the lines drawn in the cells shown in A and in other not-shown cells. ER1/MT1-ER5/MT5: profiles for mock bulk-microinjected cells. ER6/MT6-ER10/MT10: profiles for myr-p22 bulk-microinjected cells. ER11/MT11-ER15/MT15: profiles for myr-E134A-p22 bulk-microinjected cells.

bulk microinjected with myr-p22 and in neighboring non-bulk–microinjected cells, suggesting that myr-p22 induced changes concern mainly the early secretory pathway (our unpublished data).

These results suggest that raising the intracellular amount of p22 affects the organization of the ER network in two distinct manners. One, independent of p22's ability to undergo Ca^{2+}-mediated conformational changes, leads to the retraction of the ER network toward microtubule bundles. Another, dependent of p22's ability to undergo Ca^{2+}-mediated conformational changes, affects the formation of the ER network.

DISCUSSION

p22 is an EF-hand Ca^{2+}-binding protein that has been shown to undergo Ca^{2+}-mediated conformational changes (Barroso *et al*., 1996). Based on the results reported here and on the general role of EF-hand proteins as Ca^{2+} sensors, we propose that p22 transduces Ca^{2+} signals to downstream partners to subsequently regulate the assembly and organization of the ER network. Here, we also show that p22 regulates microtubule organization and dynamics independently of its ability to undergo Ca^{2+}-dependent conformational changes.

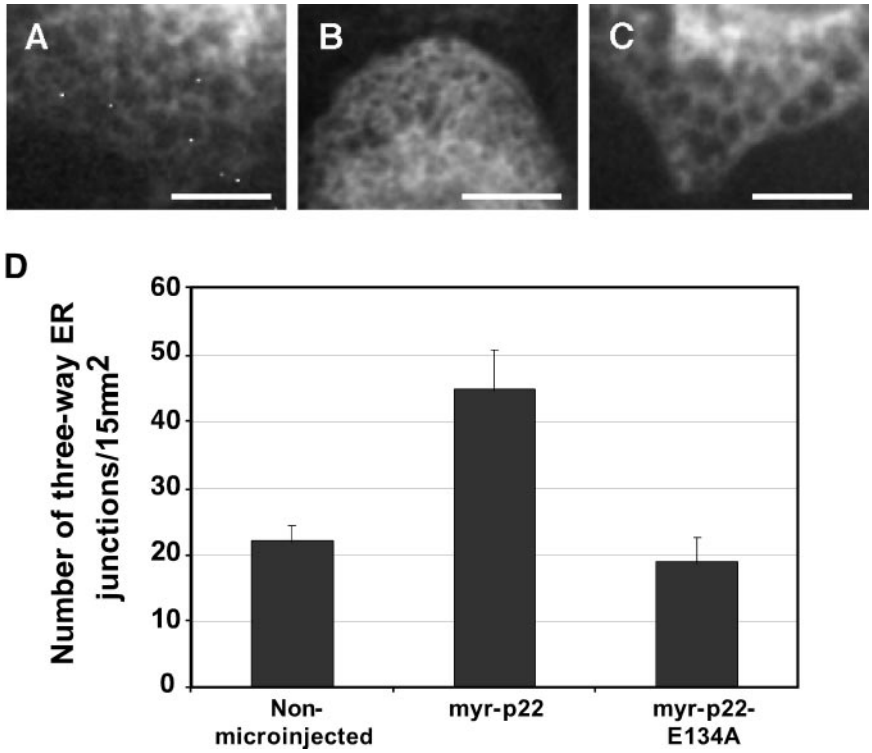

Figure 9. Effect of bulk microinjection of myr-p22 or myr-p22-E134A on ER network formation. BHK-ER cells were mock (A), myr-p22 (B), or myr-E134A-p22 (C) bulk microinjected, allowed to recover for 2 h, processed for immunofluorescence, and analyzed by confocal microscopy. A–C are representative images showing ECFP-ER fluorescence pattern in areas free of microtubule bundles. Bars, 10 μm. (D) Using ImageJ software, the number of three-way ER junctions was counted by confocal microscopy in several 15-μm^2 regions of interest (n = 11–25) as a parameter of ER network formation in vivo. Data represents mean ± SD (n = 11–25).

Role of p22 in Microtubule Organization and Dynamics

The bulk microinjection of APpep2 antibodies into BHK cells results in the removal of p22 from microtubules, leading to the fragmentation and depolymerization of the microtubule network. The amount of polymerized tubulin is reduced to ~26% at 2 h, and microtubules are practically undetectable at 4 h after APpep2 bulk microinjection. A similar phenomenon has been observed in cells microinjected with XKCM1, a microtubule-destabilizing kinesin (Kline-Smith and Walczak, 2002). It has been suggested that the significant reduction in intracellular tubulin staining detected in XKCM1-microinjected cells is due to the autoregulation of tubulin expression; increase in unpolymerized tubulin subunits leads to suppression of tubulin transcription (Kline-Smith and Walczak, 2002). In agreement with a role of p22 in microtubule stability, bulk microinjection of myr-p22 induces the formation of microtubule bundles positive for p22. Overexpression of several microtubule-binding proteins, including EB1, dynactin subunit $p150_{Glued}$, and CLIP-170, has been shown to induce the formation of microtubule bundles (Pierre *et al*., 1994; Ligon *et al*., 2003). However, these microtubule bundles are different from those induced by myr-p22, which are medium sized and distributed throughout the cell. Myr-p22–induced microtubule bundles are more similar to those induced by the overexpression of doublecortin, a microtubule-binding protein, which has been implicated in X-linked lissencephaly, a severe brain malformation affecting males (Horesh *et al*., 1999).

Microtubule bundle formation was shown to be independent of Ca^{2+}-induced conformational changes, because bulk microinjection of myr-p22-E134A also induces microtubule bundling. These data agree with previous results showing that myr-p22-E134A and myr-p22 bind microtubule pellets at similar levels and that p22–microtubule association occurs in a Ca^{2+}-independent manner in vitro (Timm *et al*., 1999). Other EF-hand proteins have also been shown to associate with different target molecules in a Ca^{2+}-independent manner. Calmodulin interacts with the small conductance Ca^{2+}-activated potassium channels (Jurado *et al*., 1999; Keen *et al*., 1999) and guanylyl cyclase-activating protein 1, a photoreceptor-specific Ca^{2+}-binding protein, binds to the microtubule-associated retina-specific guanylyl cyclase (Schrem *et al*., 1999) in a Ca^{2+}-independent manner.

p22 Associates with Membranes of the Early Secretory Pathway in an N-Myristoylation- and Ca^{2+}-dependent Manner

The requirement for p22 in membrane traffic suggests that p22 interacts with membrane-bound organelles (Barroso *et al*., 1996). Three main criteria were used to demonstrate that p22 associates with membranes of the early secretory pathway, in particular with ER membranes. First, p22 is found associated predominantly with ER (~75%) and partially with Golgi (~15%) membrane fractions by using iodixanol gradients. Second, the intracellular distribution of p22 overlaps predominantly with that of the microtubule network and partially with that of ER and Golgi apparatus. Third, p22 and an ER marker partially colocalize in punctate structures upon microtubule depolymerization. The apparent contradiction between p22's subcellular localization detected by subcellular fractionation and immunofluorescence assays is probably due to the level of microtubule polymerization during these methods; microtubules depolymerize during homogenization conditions but not during cell fixation conditions. p22's association with intracellular membranes was further confirmed by its ability to bind microsomal membranes with 40–50% efficiency and to act as a peripherally associated membrane protein.

Here, we report that p22 associates with ER membranes in vitro and under artificial conditions. However, only a minor fraction of p22 has been shown to localize to ER membranes in normal, unperturbed cells. The difficulty to see the inter-

actions between p22 and ER membranes in vivo strongly suggests that they occur in a transient, highly regulated manner.

The inability to detect p22 in endocytic membranes may indicate that the cell-free transport assay that was used to demonstrate the requirement for p22 in membrane traffic does not actually reconstitute the targeting/fusion of transcytotic vesicles with apical plasma membrane (Barroso *et al*., 1996). Alternatively, a different isoform of p22 may be required in the transcytotic targeting/fusion assay. Because p115, which was also shown to be required in the transcytotic targeting/fusion assay (Barroso *et al*., 1995), has a clear role in ER-to-Golgi transport (Nelson *et al*., 1998; Alvarez *et al*., 1999), it is possible that this assay preferentially measures membrane transport steps between the ER and the Golgi apparatus. Irrespective, the essential role of p115 in ER-to-Golgi transport confirms the ability of the cell-free targeting/fusion assay to evaluate specific protein requirements in membrane traffic, independently of its specificity.

Our results suggest that p22 interacts with membranes and microtubules by using distinct mechanisms. Two main lines of evidence support this hypothesis. First, *N*-myristoylation is required for the p22-microtubule association but not for the constitutive p22–membrane interactions. Second, Ca^{2+}-mediated conformational changes are required to stimulate p22's association with membranes over constitutive binding, but they do not lead to increased microtubule association (Timm *et al*., 1999). Furthermore, these results suggest that p22-membrane but not p22–microtubule interactions are modulated by an *N*-myristoyl-Ca^{2+} switch.

The *N*-myristoyl-Ca^{2+} switch concept was developed to describe the changes underwent by recoverin's three-dimensional structure upon binding of Ca^{2+} (Ames *et al*., 1997). In Ca^{2+}-free recoverin, the N-myristoyl group is buried within a hydrophobic pocket formed by residues from EF-1 and other helices (Tanaka *et al*., 1995). In Ca^{2+}-bound recoverin, the *N*-myristoyl group "flips out" into the aqueous solution to insert into the membranes (Ames *et al*., 1997). This model does not apply to all EF-hand proteins in a stringent manner; for example, VILIP-1, another member of the neuronal Ca^{2+}-sensor subfamily, associates with membranes independently of Ca^{2+} and undergoes a Ca^{2+}- and myristoyl-dependent increase of its ability to associate with membranes, which is suggestive of a Ca^{2+}-myristoyl switch (Lenz *et al*., 1996; Spilker *et al*., 1997, 2000, 2002a,b).

Considering the results presented here and the similarity between the structures of p22, recoverin, and VILIP-1, we propose that p22 undergoes a nonclassical *N*-myristoyl-Ca^{2+} switch to modulate its association with membranes. Exposure of the *N*-myristoyl group upon binding of Ca^{2+} and its subsequent interaction with membranes should explain the increased p22-membrane binding in the presence of Ca^{2+}.

p22 can undergo Ca^{2+}-mediated conformational changes at physiological concentrations of Ca^{2+} (>1 μM free Ca^{2+}) (Barroso *et al*., 1996). Here, we show that the p22-membrane association is significantly increased in the presence of 10 μM free Ca^{2+}. Whereas other NCS proteins, such as recoverin and VILIP-1, show a 1–2 μM Ca^{2+}-binding affinity for their ability to associate with membranes, calmodulin shows a 10-fold lower Ca^{2+}-binding affinity (Zozulya and Stryer, 1992; Burgoyne and Weiss, 2001). Although further studies are needed to clearly define p22's Ca^{2+}-binding characteristics, our data suggest that p22 is closer to calmodulin's Ca^{2+}-binding behavior than that to recoverin's. p22 is found associated with ER membranes, which can act as Ca^{2+} stores and have been shown to release large amounts of Ca^{2+} upon stimulation. Thus, we propose that p22 may be exposed to increased Ca^{2+} concentrations that would allow it to undergo Ca^{2+}-mediated conformational changes and transduce changes in intracellular Ca^{2+} levels.

p22 Facilitates the Interactions between ER Membranes and Microtubules

Three lines of evidence suggest that p22 facilitates the interactions between ER membranes and microtubule cytoskeleton. First, p22 associates with enriched ER membrane fractions and with microtubules in vivo and in vitro. Second, a two-step microtubule-membrane binding assay has shown that p22 promotes the association of ER membranes with microtubules. The p22-dependent increase in the amount of membranes bound to microtubules may be underestimated, due to the presence of endogenous p22 in the cytosol. Third, ER membrane structures seem to accumulate at myr-p22–induced microtubule bundles. Currently, we cannot distinguish whether this effect is due to ability of p22 to induce microtubule bundling, affect the organization of the ER network, or both.

Although, the formation and maintenance of the ER network occurs in a microtubule-independent manner (Dreier and Rapoport, 2000; Terasaki, 2000), ER dynamics, including ER tubule extension, may be achieved by microtubule-based mechanisms (Waterman-Storer and Salmon, 1998; Lane and Allan, 1999). Because p22 facilitates ER–microtubule interactions, it is a good candidate to modulate microtubule-dependent ER dynamics.

The results obtained using the two-step membrane-microtubule binding assay suggest that p22 facilitates the interactions between ER membranes and microtubules in a Ca^{2+}-dependent manner. However, both myr-p22 and myr-p22-E134A–induced stable microtubule bundles have been shown to accumulate ER membrane structures. Other assays specifically addressing the quantitative measurement of membrane–microtubule interactions in vivo are needed to clarify the requirement for p22's Ca^{2+}-mediated conformational changes in these intracellular events.

p22 Plays a Role in the Organization of the ER Network

A role for p22 in ER network formation is suggested by the ability of APpep2 antibodies to induce the fragmentation of ER tubules. Because APpep2 antibodies also cause microtubule fragmentation and depolymerization, we have compared their effect on the organization of the ER network with that of nocodazole, a microtubule-depolymerizing agent. Although both nocodazole and APpep2 antibodies induce microtubule depolymerization, their effects on ER organization are clearly distinct; whereas nocodazole treatment results in the retraction of the ER network toward the perinuclear region as described previously (Terasaki *et al*., 1986; Lee *et al*., 1989; Terasaki and Reese, 1994; Voeltz *et al*., 2002), introducing APpep2 antibodies into cells causes the breakage of ER tubules into punctate structures distributed throughout the cell periphery. Here, we propose that the APpep2-mediated disruption of the ER network is the combined/synergistic result of microtubule depolymerization and inhibition of ER network formation. Further supporting a Ca^{2+}-dependent role for p22 in ER network formation, we have shown that raising the amount of myr-p22, but not of myr-p22-E134A, increases significantly the number of three-way ER junctions. Several p22 functions seem to depend on its ability to undergo Ca^{2+}-mediated conformational changes. The Ca^{2+} requirement for p22's ability to associate with microsomal membranes and modulate ER network

formation and membrane trafficking events, suggests that all of these events are functionally related.

An in vitro assay for the formation of the ER has shown that membrane tubule and network formation, quantified by counting the number of three-way ER junctions, is dependent on ATP and GTP, cytosolic factors, and Ca^{2+}, and it is independent of microtubules (Dreier and Rapoport, 2000; Voeltz *et al*., 2002). Injection of antibodies against VCIP135, an essential factor for p97/p47-mediated ER membrane fusion causes a significant decrease in the number of three-way ER junctions, probably by inhibiting ER homotypic membrane fusion (Uchiyama *et al*., 2002). We propose that the Ca^{2+} dependency of p22-membrane association is involved in the Ca^{2+}-dependent ability of p22 to modulate ER network formation, probably by affecting ER tubulation and/or membrane fusion.

Together, these results suggest that p22 plays a role in microtubule organization and dynamics, microtubule–ER membrane interactions, and ER network formation. Ca^{2+}-binding and Ca^{2+}-mediated conformational changes seem to be required for p22's role in ER network formation but not for its ability to modulate microtubule organization and dynamics, suggesting at least two distinct intracellular functions for p22.

ACKNOWLEDGMENTS

We thank Amy Vroom and Mary Harp for producing and purifying recombinant, bacterially expressed p22 proteins. We also thank Drs. S. Mateer and M. King for help with image collection, as well as Wilson McIvor for assistance with HPLC protein chromatography. We also thank Dr. K. Howell, G. Bloom, Dr. E. Stzul, and Dr. B. Storrie for critically reading the manuscript. Last, we thank Drs. K. Pfister, R. Bloodgood, D. Schafer, K. Kozminski, G. Bloom, and members of the respective laboratories for insightful discussions and critical advice. This work was supported by the grant RO1-GM57519 from the National Institutes of Health.

REFERENCES

Allan, V.J., and Schroer, T.A. (1999). Membrane motors. Curr. Opin. Cell Biol. *11*, 476–482.

Alvarez, C., Fujita, H., Hubbard, A., and Sztul, E. (1999). ER to Golgi transport: requirement for p115 at a pre-Golgi VTC stage. J. Cell Biol. *147*, 1205–1222.

Ames, J.B., Ishima, R., Tanaka, T., Gordon, J.I., Stryer, L., and Ikura, M. (1997). Molecular mechanics of calcium-myristoyl switches. Nature *389*, 198–202.

Apodaca, G. (2001). Endocytic traffic in polarized epithelial cells: role of the actin and microtubule cytoskeleton. Traffic *2*, 149–159.

Ashby, M.C., and Tepikin, A.V. (2002). Polarized calcium and calmodulin signaling in secretory epithelia. Physiol. Rev. *82*, 701–34.

Barroso, M., Nelson, D.S., and Sztul, E. (1995). Transcytosis-associated protein (TAP)/p115 is a general fusion factor required for binding of vesicles to acceptor membranes. Proc. Natl. Acad. Sci. USA *92*, 527–531.

Barroso, M.R., Bernd, K.K., DeWitt, N.D., Chang, A., Mills, K., and Sztul, E.S. (1996). A novel Ca^{2+}-binding protein, p22, is required for constitutive membrane traffic. J. Biol. Chem. *271*, 10183–10187.

Bauerfeind, R., Galli, T., and De Camilli, P. (1996). Molecular mechanisms in synaptic vesicle recycling. J. Neurocytol. *25*, 701–715.

Baumann, O., and Walz, B. (2001). Endoplasmic reticulum of animal cells and its organization into structural and functional domains. Int. Rev. Cytol. *205*, 149–214.

Burgoyne, R.D., and Weiss, J.L. (2001). The neuronal calcium sensor family of Ca2+-binding proteins. Biochem. J. *353*, 1–12.

Cassimeris, L., and Spittle, C. (2001). Regulation of microtubule-associated proteins. Int. Rev. Cytol. *210*, 163–226.

Charrasse, S., Schroeder, M., Gauthier-Rouviere, C., Ango, F., Cassimeris, L., Gard, D.L., and Larroque, C. (1998). The TOGp protein is a new human microtubule-associated protein homologous to the *Xenopus* XMAP215. J. Cell Sci. *111*, 1371–1383.

Chen, J.L., Ahluwalia, J.P., and Stamnes, M. (2002). Selective effects of calcium chelators on anterograde and retrograde protein transport in the cell. J. Biol. Chem. *277*, 35682–35687.

Dreier, L., and Rapoport, T.A. (2000). In vitro formation of the endoplasmic reticulum occurs independently of microtubules by a controlled fusion reaction. J. Cell Biol. *148*, 883–898.

Fiskum, G., Craig, S.W., Decker, G.L., and Lehninger, A.L. (1980). The cytoskeleton of digitonin-treated rat hepatocytes. Proc. Natl. Acad. Sci. USA *77*, 3430–3434.

Fullerton, A.T., Bau, M.Y., Conrad, P.A., and Bloom, G.S. (1998). In vitro reconstitution of microtubule plus end-directed, GTPgammaS-sensitive motility of Golgi membranes. Mol. Biol. Cell *9*, 2699–2714.

Gravotta, D., Adesnik, M., and Sabatini, D.D. (1990). Transport of influenza HA from the trans-Golgi network to the apical surface of MDCK cells permeabilized in their basolateral plasma membranes: energy dependence and involvement of GTP-binding proteins. J. Cell Biol. *111*, 2893–2908.

Hammer, J.A., 3rd, and Wu, X.S. (2002). Rabs grab motors: defining the connections between Rab GTPases and motor proteins. Curr. Opin. Cell Biol. *14*, 69–75.

Hardham, A.R., and Gunning, B.E. (1978). Structure of cortical microtubule arrays in plant cells. J. Cell Biol. *77*, 14–34.

Henriquez, J.P., Cambiazo, V., and Maccioni, R.B. (1996). Tubulin domains for the interaction of microtubule associated protein DMAP-85 from *Drosophila melanogaster*. Mol. Cell. Biochem. *158*, 149–159.

Horesh, D., Sapir, T., Francis, F., Wolf, S.G., Caspi, M., Elbaum, M., Chelly, J., and Reiner, O. (1999). Doublecortin, a stabilizer of microtubules. Hum. Mol. Genet. *8*, 1599–1610.

Howard, J., and Hyman, A.A. (2003). Dynamics and mechanics of the microtubule plus end. Nature *422*, 753–758.

Ikura, M. (1996). Calcium binding and conformational response in EF-hand proteins. Trends Biochem. Sci**.** *21*, 14–17.

Ivessa, N.E., De Lemos-Chiarandini, C., Gravotta, D., Sabatini, D.D., and Kreibich, G. (1995). The Brefeldin A-induced retrograde transport from the Golgi apparatus to the endoplasmic reticulum depends on calcium sequestered to intracellular stores. J. Biol. Chem. *270*, 25960–7.

Ivings, L., Pennington, S.R., Jenkins, R., Weiss, J.L., and Burgoyne, R.D. (2002). Identification of Ca^{2+}-dependent binding partners for the neuronal calcium sensor protein neurocalcin delta: interaction with actin, clathrin, and tubulin. Biochem. J. *1*, 599–608.

Jurado, L.A., Chockalingam, P.S., and Jarrett, H.W. (1999). Apocalmodulin. Physiol. Rev. *79*, 661–682.

Karcher, R.L., Deacon, S.W., and Gelfand, V.I. (2002). Motor-cargo interactions: the key to transport specificity. Trends Cell Biol. *12*, 21–27.

Keen, J.E., Khawaled, R., Farrens, D.L., Neelands, T., Rivard, A., Bond, C.T., Janowsky, A., Fakler, B., Adelman, J.P., and Maylie, J. (1999). Domains responsible for constitutive and Ca^{2+}-dependent interactions between calmodulin and small conductance Ca^{2+}-activated potassium channels. J. Neurosci. *19*, 8830–8838.

Kline-Smith, S.L., and Walczak, C.E. (2002). The microtubule-destabilizing kinesin XKCM1 regulates microtubule dynamic instability in cells. Mol. Biol. Cell *13*, 2718–2731.

Klopfenstein, D.R., Kappeler, F., and Hauri, H.P. (1998). A novel direct interaction of endoplasmic reticulum with microtubules. EMBO J. *17*, 6168–6177.

Klopfenstein, D.R., Klumperman, J., Lustig, A., Kammerer, R.A., Oorschot, V., and Hauri, H.P. (2001). Subdomain-specific localization of CLIMP-63 (p63) in the endoplasmic reticulum is mediated by its luminal alpha-helical segment. J. Cell Biol. *153*, 1287–1300.

Koizumi, S., *et al*. (2002). Mechanisms underlying the neuronal calcium sensor-1-evoked enhancement of exocytosis in PC12 cells. J. Biol. Chem. *277*, 30315–30324.

Krueger, K.A., Bhatt, H., Landt, M., and Easom, R.A. (1997). Calcium-stimulated phosphorylation of MAP-2 in pancreatic betaTC3-cells is mediated by Ca^{2+}/calmodulin-dependent kinase II. J. Biol. Chem. *272*, 27464–27469.

Lane, J.D., and Allan, V.J. (1999). Microtubule-based ER motility in *Xenopus laevis*: activation of membrane-associated kinesin during development. Mol. Biol. Cell *10*, 1909–1922.

Lee, C., Ferguson, M., and Chen, L.B. (1989). Construction of the endoplasmic reticulum. J. Cell Biol. *109*, 2045–55.

Lenz, S.E., Braunewell, K.H., Weise, C., Nedlina-Chittka, A., and Gundelfinger, E.D. (1996). The neuronal EF-hand Ca(2+)-binding protein VILIP: interaction with cell membrane and actin-based cytoskeleton. Biochem. Biophys. Res. Commun. *225*, 1078–1083.

Ligon, L.A., Shelly, S.S., Tokito, M., and Holzbaur, E.L. (2003). The microtubule plus-end proteins EB1 and dynactin have differential effects on microtubule polymerization. Mol. Biol. Cell *14*, 1405–1417.

Lin, X., and Barber, D.L. (1996). A calcineurin homologous protein inhibits GTPase-stimulated Na-H exchange. Proc. Natl. Acad. Sci. USA *93*, 12631–12636.

Lin, X., Sikkink, R.A., Rusnak, F., and Barber, D.L. (1999). Inhibition of calcineurin phosphatase activity by a calcineurin B homologous protein. J. Biol. Chem. *274*, 36125–36131.

Linstedt, A.D., Mehta, A., Suhan, J., Reggio, H., and Hauri, H.P. (1997). Sequence and overexpression of GPP130/GIMPc: evidence for saturable pH-sensitive targeting of a type II early Golgi membrane protein. Mol. Biol. Cell *8*, 1073–1087.

Marsh, B.J., Mastronarde, D.N., Buttle, K.F., Howell, K.E., and McIntosh, J.R. (2001). Organellar relationships in the Golgi region of the pancreatic beta cell line, HIT-T15, visualized by high resolution electron tomography. Proc. Natl. Acad. Sci. USA *98*, 2399–2406.

McFerran, B.W., Weiss, J.L., and Burgoyne, R.D. (1999). Neuronal Ca^{2+} sensor 1. Characterization of the myristoylated protein, its cellular effects in permeabilized adrenal chromaffin cells, Ca^{2+}-independent membrane association, and interaction with binding proteins, suggesting a role in rapid Ca^{2+} signal transduction. J. Biol. Chem. *274*, 30258–30265.

Mithieux, G., and Rousset, B. (1988). Regulation of the microtubule-lysosome interaction: activation by Mg^{2+} and inhibition by ATP. Biochim. Biophys. Acta *971*, 29–37.

Mohrmann, K., Gerez, L., Oorschot, V., Klumperman, J., and van der Sluijs, P. (2002). Rab4 function in membrane recycling from early endosomes depends on a membrane to cytoplasm cycle. J. Biol. Chem. *277*, 32029–32035.

Mora, S., Durham, P.L., Smith, J.R., Russo, A.F., Jeromin, A., and Pessin, J.E. (2002). NCS-1 inhibits insulin-stimulated GLUT4 translocation in 3T3L1 adipocytes through a phosphatidylinositol 4-kinase-dependent pathway. J. Biol. Chem. *277*, 27494–27500.

Nakamura, N., Rabouille, C., Watson, R., Nilsson, T., Hui, N., Slusarewicz, P., Kreis, T.E., and Warren, G. (1995). Characterization of a cis-Golgi matrix protein, GM130. J. Cell Biol. *131*, 1715–1726.

Nelson, D.S., Alvarez, C., Gao, Y.S., Garcia-Mata, R., Fialkowski, E., and Sztul, E. (1998). The membrane transport factor TAP/p115 cycles between the Golgi and earlier secretory compartments and contains distinct domains required for its localization and function. J. Cell Biol. *143*, 319–331.

Nelson, M.R., and Chazin, W.J. (1998). Structures of EF-hand Ca^{2+}-binding proteins: diversity in the organization, packing and response to Ca^{2+} binding. Biometals *11*, 297–318.

O'Callaghan, D.W., Ivings, L., Weiss, J.L., Ashby, M.C., Tepikin, A.V., and Burgoyne, R.D. (2002). Differential use of myristoyl groups on neuronal calcium sensor proteins as a determinant of spatio-temporal aspects of Ca^{2+} signal transduction. J. Biol. Chem. *277*, 14227–14237.

Okorokov, L.A., Silva, F.E., and Okorokova Facanha, A.L. (2001). Ca^{2+} and H^+ homeostasis in fission yeast: a role of Ca^{2+}/H^+ exchange and distinct V-H^+-ATPases of the secretory pathway organelles. FEBS Lett. *505*, 321–324.

Pan, C.Y., Jeromin, A., Lundstrom, K., Yoo, S.H., Roder, J., and Fox, A.P. (2002). Alterations in exocytosis induced by neuronal Ca^{2+} sensor-1 in bovine chromaffin cells. J. Neurosci. *22*, 2427–2433.

Pang, T., Su, X., Wakabayashi, S., and Shigekawa, M. (2001). Calcineurin homologous protein as an essential cofactor for Na^+/H^+ exchangers. J. Biol. Chem. *276*, 17367–17372.

Perez, F., Pernet-Gallay, K., Nizak, C., Goodson, H.V., Kreis, T.E., and Goud, B. (2002). CLIPR-59, a new trans-Golgi/TGN cytoplasmic linker protein belonging to the CLIP-170 family. J. Cell Biol. *156*, 631–642.

Pernet-Gallay, K., Antony, C., Johannes, L., Bornens, M., Goud, B., and Rios, R.M. (2002). The overexpression of GMAP-210 blocks anterograde and retrograde transport between the ER and the Golgi apparatus. Traffic *3*, 822–832.

Peters, C., Bayer, M.J., Buhler, S., Andersen, J. S. Mann, M., and Mayer, A. (2001). Trans-complex formation by proteolipid channels in the terminal phase of membrane fusion. Nature *409*, 581–588.

Petersen, O.H., Tepikin, A., and Park, M.K. (2001). The endoplasmic reticulum: one continuous or several separate Ca^{2+} stores? Trends Neurosci. *24*, 271–276.

Pierre, P., Pepperkok, R., and Kreis, T.E. (1994). Molecular characterization of two functional domains of CLIP-170 in vivo. J. Cell Sci. *107*, 1909–1920.

Pinton, P., Pozzan. T., and Rizzuto, R. (1998). The Golgi apparatus is an inositol 1, 4, 5-trisphosphate-sensitive Ca^{2+} store, with functional properties distinct from those of the endoplasmic reticulum. EMBO J. *17*, 5298–5308.

Porat, A., and Elazar, Z. (2000). Regulation of intra-Golgi membrane transport by calcium. J. Biol. Chem. *275*, 29233–29237.

Pryor, P.R., Mullock, B.M., Bright, N.A., Gray, S.R., and Luzio, J.P. (2000). The role of intraorganellar Ca^{2+} in late endosome-lysosome heterotypic fusion and in the reformation of lysosomes from hybrid organelles. J. Cell Biol. *149*, 1053–1062.

Rappaport, L., Oliviero, P., and Samuel, J.L. (1998). Cytoskeleton and mitochondrial morphology and function. Mol. Cell Biochem. *184*, 101–105.

Scheel, J., and Kreis, T.E. (1998). Magnetic bead assay for characterization of microtubule-membrane interactions. Methods Enzymol. *298*, 381–389.

Schrag, J.D., Bergeron, J.J., Li, Y., Borisova, S., Hahn, M., Thomas, D.Y., and Cygler, M. (2001). The structure of calnexin, an ER chaperone involved in quality control of protein folding. Mol. Cell *8*, 633–644.

Schrem, A., Lange, C., Beyermann, M., and Koch, K.W. (1999). Identification of a domain in guanylyl cyclase-activating protein 1 that interacts with a complex of guanylyl cyclase and tubulin in photoreceptors. J. Biol. Chem. *274*, 6244–6249.

Schuyler, S.C., and Pellman, D. (2001). Microtubule "plus-end-tracking proteins": The end is just the beginning. Cell *105*, 421–424.

Sheff, D.R., Daro, E.A., Hull, M., and Mellman, I. (1999). The receptor recycling pathway contains two distinct populations of early endosomes with different sorting functions. J. Cell Biol. *145*, 123–139.

Spilker, C., Dresbach, T., and Braunewell, K.H. (2002a). Reversible translocation and activity-dependent localization of the calcium-myristoyl switch protein VILIP-1 to different membrane compartments in living hippocampal neurons. J. Neurosci. *22*, 7331–7339.

Spilker, C., Gundelfinger, E.D., and Braunewell, K.H. (2002b). Evidence for different functional properties of the neuronal calcium sensor proteins VILIP-1 and VILIP-3, from subcellular localization to cellular function. Biochim. Biophys. Acta *1600*, 118–127.

Spilker, C., Gundelfinger, E.D., and Braunewell, K.H. (1997). Calcium- and myristoyl-dependent subcellular localization of the neuronal calcium-binding protein VILIP in transfected PC12 cells. Neurosci. Lett. *225*, 126–128.

Spilker, C., Richter, K., Smalla, K.H., Manahan-Vaughan, D., Gundelfinger, E.D., and Braunewell, K.H. (2000). The neuronal EF-hand calcium-binding protein visinin-like protein-3 is expressed in cerebellar Purkinje cells and shows a calcium-dependent membrane association. Neuroscience *96*, 121–9.

Spira, M.E., Oren, R., Dormann, A., Ilouz, N., and Lev, S. (2001). Calcium, protease activation, and cytoskeleton remodeling underlie growth cone formation and neuronal regeneration. Cell. Mol. Neurobiol. *21*, 591–604.

Tanaka, T., Ames, J.B., Harvey, T.S., Stryer, L., and Ikura, M. (1995). Sequestration of the membrane-targeting myristoyl group of recoverin in the calcium-free state. Nature *376*, 444–447.

Terasaki, M. (2000). Dynamics of the endoplasmic reticulum and Golgi apparatus during early sea urchin development. Mol. Biol. Cell *11*, 897–914.

Terasaki, M., and Reese, T.S. (1994). Interactions among endoplasmic reticulum, microtubules, and retrograde movements of the cell surface. Cell Motil. Cytoskeleton *29*, 291–300.

Terasaki, M., Chen, L.B., and Fujiwara, K. (1986). Microtubules and the endoplasmic reticulum are highly interdependent structures. J. Cell Biol. *103*, 1557–68.

Thyberg, J., and Moskalewski, S. (1999). Role of microtubules in the organization of the Golgi complex. Exp. Cell Res. *246*, 263–279.

Timm, S., Titus, B., Bernd, K., and Barroso, M. (1999). The EF-hand Ca^{2+}-binding protein p22 associates with microtubules in an N-myristoylation-dependent manner. Mol. Biol. Cell *10*, 3473–3488.

Uchiyama, K., *et al*. (2002). VCIP135, a novel essential factor for p97/p47-mediated membrane fusion, is required for Golgi and ER assembly in vivo. J. Cell Biol. *159*, 855–866.

van der Sluijs, P., Hull, M., Zahraoui, A., Tavitian, A., Goud, B., and Mellman, I. (1991). The small GTP-binding protein rab4 is associated with early endosomes. Proc. Natl. Acad. Sci. USA *88*, 6313–6317.

Voeltz, G.K., Rolls, M.M., and Rapoport, T.A. (2002). Structural organization of the endoplasmic reticulum. EMBO Rep. *3*, 944–950.

Walenta, J.H., Didier, A.J., Liu, X., and Kramer, H. (2001). The Golgi-associated hook3 protein is a member of a novel family of microtubule-binding proteins. J. Cell Biol. *152*, 923–934.

Waterman-Storer, C.M., and Salmon, E.D. (1998). ER membrane tubules are distributed by microtubules in living cells using three distinct mechanisms. Curr. Biol. *14*, 798–806.

Zozulya, S., and Stryer, L. (1992). Calcium-myristoyl protein switch. Proc. Natl. Acad. Sci. USA *89*, 11569–11573.